The Superconducting Super Collider

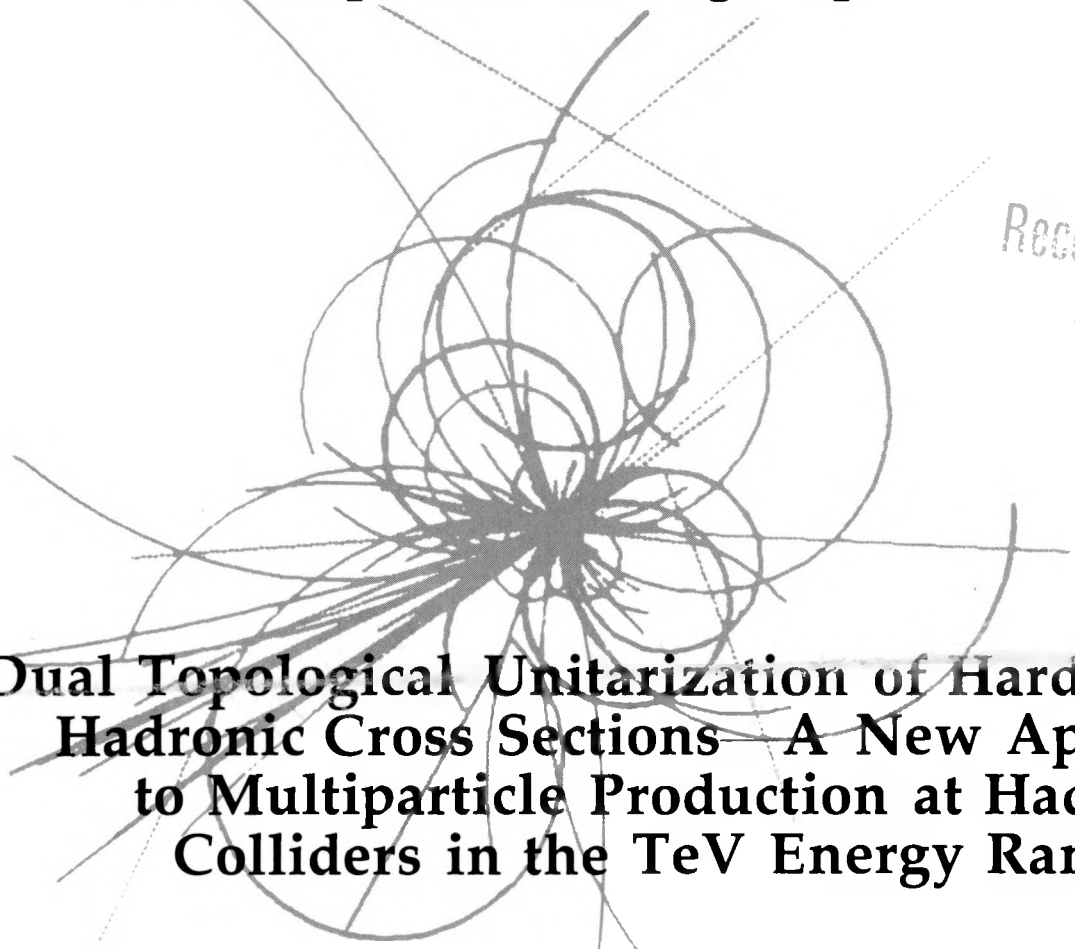

Dual Topological Unitarization of Hard and Soft Hadronic Cross Sections—A New Approach to Multiparticle Production at Hadron Colliders in the TeV Energy Range

J. Ranft, P. Aurenche, F. Bopp, A. Capella, K. Hahn, J. Kwiecinski, P. Maire, and J. Tran Thanh Van

SSC Central Design Group

December 1987

SSC--149

DE90 013764

DUAL TOPOLOGICAL UNITARIZATION OF HARD AND SOFT HADRONIC CROSS SECTIONS, A NEW APPROACH TO MULTIPARTICLE PRODUCTION AT HADRON COLLIDERS IN THE TeV ENERGY RANGE

J. Ranft, K. Hahn
Lawrence Berkeley Laboratory
1 Cyclotron Road, Berkeley California USA 94720

and

P. Aurenche, P. Maire
LAPP, Lab. d'Annecy-le-Vieux de Phys. des Particles
Chemin de Bellevue - BP 909, F-74019 Annecy-le-Vieux CEDEX France

and

F. Bopp
Univ. of Siegen, FB Phys., Adolf-Reichwein-Str 2
P. O. Box 10 12 40, D-5900 Siegen Federal Republic of Germany

and

A. Capella, J. Tran Thanh Van
Lab. de Phys. Theor. et Particules Elementaries
Univ. de Paris-Sud, Batiment 211, F-91405 Orsay France

and

J. Kwiecinski
Krakow Inst. of Nuclear Physics
High Energy Lab, ul. Kawiory 26 A, PL-30-055 Krakow Poland

December 1987

SSC-149

December 1987

Dual Topological Unitarization of Hard and Soft Hadronic Cross Sections, A New Approach to Multiparticle Production at Hadron Colliders in the TeV Energy Range

J. Ranft,* P. Aurenche,† F. Bopp,° A. Capella,ᶻ K. Hahn,*
J. Kwiecinski,△ P. Maire† and J. Tran Thanh Vanᶻ

Abstract

The dual topological unitarization of hard and soft hadronic collisions is formulated as a Monte-Carlo event generator for events containing both the soft (low $p_\perp$) and hard (jets, minijets) component of hadron production. The parameters of the model are determined from fits to the energy dependence of the total and inelastic hadron cross-sections and from the predictions of the QCD-parton model for the perturbative hard constituent scattering cross sections. The properties of the model are studied. Good agreement of the model predictions is found with data at present accelerator and collider energies. The predictions of the model for TeV colliders are presented. Interesting changes of the produced multiparticle system are formed when selecting classes of events with and without hard jets or minijets.

* SSC Central Design Group, Lawrence Berkeley Laboratory, Berkeley USA. Permanent address: Sektion Physik, Karl-Marx-Universität, Leipzig, G.D.R.
† LAPP, Annecy, France
° Universität Siegen, F.R.G.
ᶻ LPTHE, Orsay, France
△ Institute of Nuclear Physics, Krakow, Poland

1. Introduction

The dual topological unitarization of hard and soft hadronic cross sections is a new model of hadronic multiparticle production.

During the last years several groups have studied soft hadronic multiparticle production in the framework of the DTU-model [1, 2, 3, 4, 5]. These models and in particular the Monte-Carlo formulation of this model in the form of the dual multi-chain fragmentation model [4, 5] belong to the starting points for the new model described here.

Experimental observations made it clear, that at collider energies the soft and hard components of hadronic multiparticle production are closely related. These observations are the discovery at the CERN-SPS-collider of correlations between the average transverse momenta of hadrons produced and the multiplicity density in rapidity [6] and the observation of 'minijets' in hadronic collisions and changes of the properties of the underlying soft events in data samples with jets or minijets [7, 8].

Both of these properties were understood within the dual multichain framentation model [5, 9] by introducing transverse momenta (in addition to intrinsic transverse momenta) with magnitudes, which could only be interpreted to be due to hard constituent scattering for the partons at the ends of the fragmenting chains.

The need for an uniform treatment of hard and soft hadronic collisions is furthermore underlined by the fact that the perturbative QCD cross sections for hard constituent scattering rise strongly with energy reaching for transverse

momenta greater than 2 GeV/c values around 200 mb at the energy of the SSC. This is larger than the total hadronic cross section at these energies. At those energies one expects that unitarity corrections should play an important role. Those corrections then inevitably lead to several semihard interactions resulting in the increase of the average number of jets.

The perturbative hard constituent scatterings are also one of the processes responsible for the rise of the hadronic cross sections. This was studied quantitatively in papers by Capella, Tran Thanh Van and Kwiecinski [10] and Durand and Pi [11] where the consequences for the total and inelastic cross sections of the unitarization of soft and hard scattering cross sections were studied. This model as formulated in [10] is the second starting point for the model to be described here.

In Section 2 the basic ideas of the model will be outlined. In Section 3 the total and inelastic hadronic cross-sections are studied within the model, compared to data at present energies and predicted in the SSC energy range. In Section 4 the properties of the two component (hard and soft) multi Pomeron events according to the model are presented. In Section 5 the model is formulated on the parton level, where the partons are understood as the quarks, antiquarks and diquarks at the ends of the hard and soft multiparticle strings. In Section 6 finally the properties of the model are presented after the fragmentation of all strings into hadrons and the decay of all hadronic resonances. The model is compared to data in the ISR and SPS collider energy range. Subclasses of events are studied with and without hard jets. In Section 7 the predictions of the model in the form of the hadronic Monte-Carlo event generator DTUJET for 40 TeV

collisions in the SSC interaction regions are presented. Such consequences can also be investigated using events generated by DTUJET. The code DTUJET is described in a SSC Report [11].

2. Unitarization of Soft and Hard Hadron Cross Sections, A Model for Hadron Cross Sections and Multiparticle Production

We start by describing shortly the dual multistring fragmentation model for soft hadron production. In first approximation the proton is made out of valence quarks q_v and diquarks qq_v. In hadronic collisions (to be definite we consider only $\bar{p}-p$ collisions) the color is rearranged between the constituents of the hadrons and two high mass color singlett chains or strings are formed $S_1 = (qq_v - \bar{q}\bar{q}_v)$ and $S_2 = (q_v - \bar{q}_v)$, see Fig. 1a. Via unitarity, the square of diagram 1a generates the imaginary part of the $\bar{p}p$ elastic amplitude, which is dominated at high energy by Pomeron exchange, see Fig. 1b.

A theoretical analysis [13, 14] of the s-channel content of this diagram shows that the Pomeron singularity is generated by the production of two heavy masses S_1 and S_2 at small transverse momentum ($p_\perp^{S_i}/M_{S_i} << 1$), overlapping in rapidity space, i.e., in the configuration of Fig. 1a, when interpreted in terms of quark diagrams. We assume further [14] as in the parton model, that the quark and diquark in the proton carry momentum fractions x_q and x_{qq}, respectively. It is then easy to determine the global properties of the strings such as the masses

$$M_1^2 = x_q x_{\bar{q}} S$$
$$M_2^2 = x_{qq} x_{\bar{q}\bar{q}} S \qquad (1)$$

where $\sqrt{s}$ is the total energy, the rapidities in the c.m.s.

$$Y_1 = \frac{1}{2} \ln x_q / x_{\bar{q}}$$
$$Y_2 = \frac{1}{2} \ln x_{qq} / x_{\bar{q}\bar{q}} \qquad (2)$$

or the quantum numbers, which are just obtained from those of the constituents.

In the next level of approximation, the effect of gluons, sea quarks and antiquarks in the incoming hadrons are taken into account. An extra $q\bar{q}$ pair in each of the colliding hadrons leads to the production of 4 strings as shown in Fig. 2. When calculating the elastic cross section, this contribution leads to two-Pomeron exchange.

The weights for the production of 2 strings (one Pomeron exchange), 4 strings (2-Pomeron exchange) and so on are related to the amplitudes for n-Pomeron exchange given by the Gribov (eikonal) model. Using the AGK cutting rules [15] one obtains the probabilities for N-cut Pomerons or equivalently 2N string production as used in the dual multichain fragmentation models [1 – 5].

At the energy of present and future hadron colliders the hard scattering of quarks and gluons as calculated in QCD perturbation theory [16] becomes a second important mechanism of multiparticle production besides the soft particle production mechanism as described above. In the QCD-parton model the cross section for hard constituent scattering is given by

$$\sigma_h(s) = \sum_{ij} \int dx_1 \int dx_2 \int d\hat{t} \, \frac{d\sigma_{ij}}{d\hat{t}} \, F_i(x_1, Q^2) \, / F_j(x_2, Q^2) \qquad (3)$$

where the $F_i(x_i Q^2)$ are the parton structure functions of the hadron and the $d\sigma_{ij}/d\hat{t}$ is the perturbative hard scattering cross section of the constituents i and

j. The cross section (3) makes sense only at scales Q^2, which are sufficiently large. In practice, this means, that the cross section (3) can only be calculated for transverse momenta of the scattered constituents (jets, minijets) greater than 2 GeV/c. Corrections due to the large gluon density [17] in such collisions are not yet important for the minijet production at energies of $\sqrt{s} = 40$ TeV [18]. We will use in this paper a minimum transverse momentum for σ_n(s) of $p_{\perp,min} = 2$ GeV/c. The dash dotted curve in Fig. 3 gives as function of the c.m.s. energy $\sqrt{s}$ the cross section σ_h as calculated for all constituent subprocesses [16] using the parameterization of the hadron structure functions as given by Eichten, Hinchliffe, Lane and Quigg [19] (EHLQ-1). This cross section rises in the energy region of interest practically as a power of s.

It should be stressed that there is considerable theoretical and experimental uncertainty about this rise of σ_h with the energy. Structure functions like the ones used here postulate a $1/x$ dependence for gluon- and sea-quark-structure functions at some reference scale ($Q_o^2 \approx 5$ GeV^2) but of course the QCD evolution makes the gluon distribution much steeper of larger Q^2 values. At the x-values of 10^{-4} which become important for the production of minijets at SSC energies, the structure functions cannot be determined experimentally at present accelerator energies and there is presently no practical method available which would permit to calculate the structure functions from QCD. It has been argued that the x dependence of the structure functions at these small x-values indeed differ from x^{-1}. Collins [20] presented arguments for a $x^{-1.5}$ behavior. The consequences of an alternative behavior of the structure functions at small x-values for the predictability of hard scattering cross sections and the production of minijets at the

energy $\sqrt{s} = 40$ TeV of the SSC collider have been discussed repeatedly [21, 22].

The simultaneous unitarization of both hadronic cross sections, the soft and the hard cross sections, was first performed in papers by Capella et al. [10] and Durand et al. [11]. In these models one has two kinds of exchanged Pomerons, soft Pomerons, corresponding to a pair of soft strings in the inelastic cross section and hard Pomerons, corresponding to two hard scattered chains.

This generalization of the AGK approach leads in our model to a decomposition of the scattering amplitude in terms of contributions with the exchange of say ℓ soft and m hard Pomerons corresponding to inelastic events with 2ℓ soft and $2m$ hard strings (large $p_\perp$ jets or minijets).

3. Unitarization of Soft and Hard Hadron Scattering and Total and Inelastic Hadron-Hadron Cross Sections

In Appendix A we give the expression obtained by Capella et al. [9] for the total and inelastic hadronic cross-sections in terms of the bare (input) hard and soft cross sections σ_h and σ_s. We use for σ_h the cross section as obtained by numerical integration of (1) and summing over all constituent subprocesses. The cross section σ_h obtained is given in Fig. 3 (dot-dashed curve).

For the soft cross sections we use [10]:

$$\sigma_s = a\, s^{\alpha - 1} \tag{4}$$

with $\alpha = 1.076$ and $a = 37.8$ mb. For σ_{TP} the expression is

$$\sigma_{TP} = c[\ln(b + 2\alpha' \ln s) - \ln(b + 2\alpha' \ln 20)] \tag{5}$$

with $\alpha' = 0.24$ GeV^{-2}, $b = 3.51$ GeV^{-2} and $c = 40$ mb. For the slopes we take $b_s = b + \alpha' \ln s$, $b_h = b$ and $b_{TP} = b_s$.

In Fig. 3 we present the total proton-proton cross section obtained from (A-1) and compare to date at energies up to cosmic ray energies near the energy of the SSC. This cross section agrees also very well with parameterizations like the ones presented by Block and Cahn [23]. We give in Fig. 3a the inelastic and elastic cross sections σ_{inel} and σ_{el} and the inelastic hadronic cross section corresponding to events with one or more than one hard jets or minijets $\sigma_{h,inel}$.

Durand and Pi [11] try to explain the rise of the total cross section only by the rise of the perturbative hard cross section σ_h. They use a constant energy independent soft input cross section

$$\sigma_s = \text{const} \quad , \quad \sigma_{TP} = 0 \tag{6}$$

and choose the cutoff momentum transfer $Q^2_{min} = 2$ (GeV/c)^2 to reproduce the cross section $\sigma_{\bar{p}p}$ as measured at the CERN-SPS-Collider. In Fig. 3b we present the results obtained using the expressions in Appendix A, a constant σ_s and the same hard cross section σ_h ($p_{\perp,min} = 2$ GeV as used for the calculation in Fig. 3a. The total cross section calculated is well below the SPS-collider data. Instead of decreasing the cut off $p_{\perp,min}$ further below 2 GeV/c we prefer the model in the form as used in Fig. 3a, where also the soft input cross section σ_s rises with energy.

It is remarkable that the cross sections $\sigma_{h,inel}$ and even σ_{inel} are smaller than the bare hard cross sections σ_h (or the bare soft cross section σ_s).

We expect in average inelastic collisions

$$\langle n_h \rangle = \sigma_h / \sigma_{inel} \tag{7}$$

hard Pomerons (2 n_h hard strings) and

$$\langle n_s \rangle = \sigma_s / \sigma_{inel} \tag{8}$$

soft Pomerons (2 n_s soft strings). Only in the fraction

$$\langle F_h \rangle = \sigma_{h,inel} / \sigma_{inel} \tag{9}$$

of all inelastic collisions jets or minijets are expected. The average number of hard Pomerons in this fraction of collisions

$$\langle n_{h,h} \rangle = \sigma_h / \sigma_{h,inel} \tag{10}$$

is even larger than $\langle n_h \rangle$.

The unitarization scheme leads to rather stable hadronic cross sections when changing the input cross sections σ_s and σ_h. If we for instance introduce a K factor $K = 1.5$ into the calculation of σ_h, we get at $\sqrt{s} = 40$ TeV an increase of σ_h from 194 mb to 291 mb. This leads to increases of σ_{tot} from 132 to 139 mb, of σ_{inel} from 88 to 90 mb and of $\sigma_{h,inel}$ from 52 to 59 mb. Such an increase would however change the structure of the inelastic events more strongly. The increase of σ_h leads roughly to an corresponding increase of the numbers of jets or minijets $\langle n_h \rangle$ and $\langle n_{h,h} \rangle$ per event.

4. The Two Component Multi-Pomeron Model for Inelastic Hadron Interactions

Due to the alternating sign of the terms with rising powers ℓ and m, the cross section σ_{inel} as given in (A-2) cannot be interpreted as a sum over cross-sections corresponding to ℓ soft and m hard Pomerons. To obtain the cross sections for n_s soft and n_h hard Pomerons, the cross section σ_{inel} in (A-2) has to be resummed into a sum with only non-negtive terms. In Appendix B such an expression is given. The cross section σ_{ij} in (B-1) is the cross section for $n_s = i$ cut soft and $n_h = j$ cut hard Pomerons. As explained in Appendix B, the corresponding formulae become transparent in the impact parameter representation.

This expression σ_{n_s,n_h} simplifies considerably if one evaluates the sum in the approximation of vanishing σ_{TP}. In the TeV-collider energy range, where we are mostly interested, this should be a good approximation since $\sigma_{TP} \ll \sigma_s, \sigma_h$. All results presented in this paper correspond to this approximation. In the energy range up to 40 TeV and with the input cross sections as given in Fig. 3 and in (2) at least the first 50 terms have to be computed in the remaining alternating sums in (B-1). This approximation might however influence the results obtained at the energy of the CERN-SPS-Collider, this will be discussed later.

Many properties of the model can be understood already at this level of multi-Pomeron cross sections. In Fig. 4 we present as function of the numbers of soft and hard Pomerons n_s and n_h the results of the Monte Carlo sampling of 1000 events at some energies between the CERN-SPS collider and the SSC.

We note, the width of the distribution as well as the average values of the numbers n_h and n_s increase with energy. At low energy, the hard cross sections σ_h and $\sigma_{h,inel}$ approach zero and we get as the low energy limit $\sigma_{inel} = \sigma_{n_s=1,n_h=0}$. With rising energies about 50% of the total inelastic cross section remains in the fraction with $n_h = 0$ (no hard scattering), but the width of the distribution in n_s, the number of soft Pomerons and the average values $\langle n_s \rangle$ increase with energy. Also for $n_h \neq 0$ the shape of the distribution in n_s becomes wider and flatter.

5. Formulation of the Model on the Level of the Partons at the End of the Strings

Up to here we have selected the main parameters of the model by choosing the input soft and hard cross sections σ_s and σ_h and obtaining a good fit to the hadronic total and inelastic cross sections. From this we obtain without further input the multi Pomeron cross-sections $\sigma_{(n_s,n_h)}$.

Next we have to choose the methods to sample the partons at the ends of the hard and soft strings in events with n_s soft and n_h hard Pomerons.

The hard scattering cross section (3) before performing the integrations and sums is just the distribution function for the x values of the partons which get engaged in the hard scattering. We need of course distribution function for n_h hard scatterings and simultaneously n_s soft scatterings.

To demonstrate, that in most situations one hard scattering corresponds to one hard Pomeron and therefore to two additional strings, we give in Fig. 5 some examples of events with one soft (valence-valence) pair of strings and one hard

scattering.* In the case, that gluons are involved in the hard scattering, we have to transform the gluons into quark-antiquark pairs before forming strings, which can fragment into hadrons. In some situations, for instance for valence quark-valence quark hard scattering, we need from each interacting proton one gluon or sea quark-antiquark pair in order to form color singlett strings involving the diquarks.

To sample the hard scattering of partons in the code DTUJET we use the method and parts of the FORTRAN-code of the Lund event generator PYTHIA [24]. We fragment gluons in the final state of the hard scattering always into quark pairs to prepare for the string fragmentation as indicated in Fig. 5.

Besides sampling the partons involved in hard scattering we have also to sample the partons at the ends of the soft strings. In an event with 2 n_s soft chains and n_h hard Pomerons (to be definite we consider as an example the case of hard gluon-gluon scattering) we have to sample the partons for each of the primary hadrons from exclusive parton distributions for 2 n_s soft (valence quark, valence diquark and $(2n_s-2)/2$ quark-antiquark pairs or gluons which fragment subsequently into quark-antiquark pairs) and n_h hard partons (gluons). This exclusive parton distribution has the form

$$\rho(x_1, ..., x_{2n_s}, x_{2n_s+1}, ..., x_{2n_s+n_h}) \sim$$
$$\frac{1}{\sqrt{x}_1}\Big(\prod_{2}^{2n_s-1}\frac{1}{x_i}\Big)\, x_{2n_s}^{1.5} \prod_{2n_s+1}^{2n_s+n_h} g(x_i)\, \delta\Big(1-\sum_{1}^{2n_s+n_h} x_i\Big) \qquad (11)$$

* One should have in mind however, that assignment of strings to a given parton configuration is ambiguous and model dependent.

The form of the soft parton distributions for small x-values is obtained by dual Regge arguments [25]. For valence partons

$$\rho(x_q) \sim \frac{1}{x_q^{\alpha_R}} \quad , \quad \alpha_R = \frac{1}{2}$$
$$f(x_{qq}) \sim \frac{1}{x_{qq}^{\alpha_E}} \quad , \quad \alpha_E = -1.5 \tag{12}$$

where α_R is the leading $(q\bar{q})$ Regge trajectory and α_E the exotic $(qq\bar{q}\bar{q})$ trajectory. The x distribution of soft sea quarks is $f(x) \sim 1/x$ for $x \to 0$. The distributions $g(x_i)$ are the distribution functions for the x values of partons from the hard scattering, they follow from (3).

In the present version of the model we do not use a method sampling exactly from (11), instead we use a rejection method, where the x values of the hard and soft partons are first sampled independently and we reject the event if the x-value remaining for the diquark is inconsistent. In the dominating configuration the valence diquarks get much larger x-values than all other partons, we find, that only very few configurations sampled by this approximate method have to be rejected. A method to sample exactly from (11) is presently being worked out.

To judge the importance of the different hadron production mechanisms in the model, we subdivide the strings and the partons at their ends into three classes. Only in some situations the subdivision is ambiguous. The three classes are:

- soft valence strings
- soft sea strings
- hard strings

In Table 1 we give the energy fractions carried by the strings (or partons) of the three classes for typical collision energies. This table indicates, that for the hard scattering cross sections σ_h as used here, the soft valence strings remain up to SSC energies the dominant mechanisms carrying around 90% of the total collision energy. This situation could however change, if the hard cross-sections σ_h rise much stronger with energy as the ones given in Fig. 3a which are used here. It was already discussed in Section 2, that a stronger rise of σ_h cannot be excluded from our present experimental and theoretical understanding of the hadron structure functions in the region $x \to 0$.

In Figs. 6a and 6b we present at $\sqrt{s} = 540$ GeV and 40 TeV distributions of the partons at the end of the three kinds of strings. It is clearly visible, that the soft valence strings remain the leading component in the TeV energy range. If at small x the structure functions would rise stronger than x^{-1}, the hard string component would rise. This component carried only about 5% of the total energy in the present formulation. One could imagine, that this component rises by a factor 10 up to carrying 50% of the collision energy before the model as formulated here would become unreliable. We will discuss later in Section 7 the consequences of such a rise on the multiplicities at 40 TeV.

6. The Properties of the Model After the Fragmentation of All Strings into Hadrons

After having selected the x-values, hard and primordial transverse momenta and flavors of all quarks, antiquarks and diquarks at the ends of the strings, the remaining task is the fragmentation of the strings into hadrons and the decay of all hadron resonances into stable hadrons.

There are more than one independent fragmentation and string fragmentation models available, which could be used. For the results reported here, we use the independent fragmentation chain decay code BAMJET [26] and the resonance decay code DECAY [27]. Figure 5 gives examples for the string structure in simple events with one hard and one soft Pomeron. In Table 2 we present average total and charged multiplicities for each of the three mechanisms as well as for the complete events. These multiplicities correspond to nondiffractive inelastic events. Diffraction is not included in the present version of the model.

In Fig. 7 we present rapidity distributions of all charged particles at energies between $\sqrt{s} \approx 20$ GeV ($E_{lab} = 200$ GeV) and $\sqrt{s} = 40$ TeV. The shape of the rapidity distribution is interesting to compare with the concept of a rapidity plateau which was popular in the seventies. Instead we find the rapidity distribution to get wider and at the same time higher. The rise in both directions is approximately proportional to $\ln s$ therefore we find a rise of the total multiplicity proportional to $\ln^2 s$. The shape of the rapidity distribution over most of the energy range looks similar to a Gaussian, only at the highest energies it is flatter in the center than a Gaussian. At the lowest energy $E_{lab} = 200$ GeV we compare

the rapidity distribution with data[28] and find a good agreement. At higher energies only pseudorapidity distributions of all charged particles are measured.

In Fig. 8 we present pseudorapidity distributions at 6 energies of past (CERN-ISR) present (CERN-SPS and Fermilab collider) and future (SSC) hadron colliders. At ISR and SPS energies we compare with data from non single-diffractive events from the UA-5 collaboration[21] and find good agreement.

In Fig. 9 we compare semi-inclusive pseudorapidity distributions at $\sqrt{s} = 200$ and 900 GeV with data from the UA-5 Collaboration[29]. In Fig. 10 we present Feynman-x distributions at $\sqrt{s} = 540$ GeV and 40 TeV. Feynman scaling is violated in the model but the deviations from Feynman scaling in the fragmentation region are small.

In Fig. 11 we present transverse momentum distributions integrated over the total longitudinal momentum or rapidity region at three energies. Again, we do not see significant changes with energy in the transverse momentum region below 5 GeV/c. The onset of hard scattering is visible in the change of the slope of the distributions with increasing transverse momentum.

Correlations between the average transverse momenta and the multiplicity per rapidity interval were found experimentally by the CERN-SPS-UA1 Collaboration[30]. In Fig. 12 we compare the model at $\sqrt{s} = 200$ to 900 GeV with the data[30] at 540 and 900 GeV. The average transverse momenta rise with the multiplicity steeper in the data than in the model. According to Table 2 only 10–15% of all charged particles in the model result from hard strings or minijets. In the model the correlation effect can only be explained by the minijet

component. The minijets have a cut-off transverse momentum of 2 GeV/c. Obviously in order to explain the full effect, we would have to give to the partons at the ends of the soft strings transverse momenta in such a way, that the total parton transverse momentum distribution becomes smooth, this is only possible, if the transverse momenta of some of the partons at the ends of the soft strings are increased. In this way also the rise of the average $p_\perp$ with multiplicity would become steeper. In the old model [5], introducing all transverse momenta of the string ends, it was shown, that good agreement can be reached.

The violation of KNO scaling [31] in multistring models of the considered type was already pointed out some 15 years ago [32]. Also in the more detailed multistring models [1 – 4], the violation of KNO scaling was studied. This violation agrees qualitatively with the one found experimentally by the UA5-Collaboration [33]. We present in Fig. 13 KNO multiplicity distributions calculated at $\sqrt{s}$ = 200, 900 GeV and 40 TeV. Over this large energy range the KNO-violation is indeed very strong. The rising tail of the distribution at large values of $n_{ch}/\langle n_{ch}\rangle$ is a signal for the production of more and more soft and hard strings with rising energy. It should be noted, that the distributions in Fig. 13 at the SPS-Collider energies while displaying the correct non-KNO behavior are still somewhat narrower than the KNO distributions found experimentally [33]. We take this as an indication, that our approximate calculation of the multi-Pomeron distribution as discussed in Section 4 might not be appropriate.

The changes of the event structure predicted by the model when selecting subclasses of events with and without hard jets [minijets] follow from the changes of the Pomeron distribution (see Fig. 4) between the regions with $n_h = 0$ and

$n_h \neq 0$. In Fig. 9 we present pseudorapidity distributions at 540 GeV obtained by selecting normal average events, events without hard jets and events with jets of a given minimum transverse momentum. In these distributions the jets are always the ones known to the model, not jets found by a jet finding mechanism. We find a dramatic rise of the plateau of the rapidity and pseudorapidity distributions when selecting events with jets. In Fig. 10 the same features of the model are shown at the energy of 40 TeV. These features of the model make it likely, that the model reproduces the rise of the plateau under the jets as determined by the jet finding algorithm of the UA-1 collaboration [7, 8].

7. Hadron Production in 40 TeV Collisions at the SSC

In Table 3 we present multiplicities of different kinds of hadrons and energy fractions carried by these kinds of hadrons calculated by the DTUJET code. Some explanations to this table: The photons result from decay channels of hadron resonances. There are neutral Kaons K_L^0, K_S^0, K^0 and $\bar{K}^0$. The K_L^0 and K_S^0 follow from some decay channels as given in the particle data tables. The K^0 and $\bar{K}^0$ are produced in BAMJET. The user should decide in which form he needs the neutral K-mesons. The table as given is for $\bar{p}p$ collisions, the only differences seen in pp-collisions are obvious changes in the baryon and antibaryon multiplicities.

In Section 5 and Table 1 we found, the jets (minijets) in the model carry less than 5% of the total energy. According to Table 2 about 25% of the total or charged multiplicity originate from these strings. In the case, that the structure functions at low x values increase faster than x^{-1} we could arrive at a situation,

where the hard strings carry 50% of the energy. This would then mean, that we get at $\sqrt{s} = 40$ TeV a total (charged) multiplicity of approximately 600 (340) or about a factor three higher than given in Table 2. We feel that such a behavior is the extreme case. We would also expect, that shadowing effects [17] become significant, when the gluon distribution becomes so big at small x. These shadowing corrections should then reduce the gluon distribution stabilizing the minijet productions. However it is easily possible, that the minijet cross section at $\sqrt{s} = 40$ TeV becomes three times bigger than the 200 mb used here. In this case the total and charged multiplicites and the maxima of the rapidity or pseudorapidity distributions would rise by approximately 50%.

In a new fit to deep inelastic scattering data Martin et al. [35] determine the quark and gluon structure functions. Their favored solution has the x^{-1} behaviour for the gluon distribution. At the x-values of interest for the minijet production at the SSC this gluon distribution nevertheless is higher than the ELHQ-distribution used here. It will be interesting to redo the calculations reported here as soon as the Martin et al. [35] structure functions become available.

In Figs. 16-18 we give pseudorapidity distributions for all particles, all hadrons, particles leading to electromagnetic cascades (π^0 and γ), all charged particles and all neutral particles. Figure 16 gives the multiplicities per pseudorapidity unit $\mathrm{dN/d}\eta$, Fig. 17 gives the energy per pseudorapidity unit $\mathrm{dE/d}\eta$ and Fig. 18 gives the total energy within the bounds $-\eta \ldots +\eta$.

In Figs. 19-20 we give similar histograms, this time as function of the polar angle θ. Figure 19 gives $\mathrm{dN/d}\Omega$ in particles per sterrad, Fig. 20 gives $\mathrm{dE/d}\Omega$ in GeV/sterrad.

In Fig. 21 we present as a scatter plot with the pseudorapidity η and the logarithm of the momentum on the two orthogonal axes some 4000 secondaries produced in 40 TeV collisions. The distribution of the secondaries in these two variables can be seen in more detail in the next figure.

In Fig. 22 we present a two dimensional histogram representing $d^2N/dpd\eta$ for 50 momentum bins and pseudorapidity bins of width $\Delta\eta = 0.5$. Figure 22 gives $d^2N/dpd\eta$ for 10 pseudorapidity bins 0–0.5, 1–1.5, etc. as function of the momentum p. In each plot the histograms are given for all particles, all hadrons and all particles leading to e.m. cascades (π^0 and γ).

We would like to point out that the code DTUJET and a writeup will be available[11]. DTUJET-87 can be used to calculate histograms like the ones presented here or to write events to a computer file to be used by other codes.

8. Summary

We have presented results from the first version of a new model for multiparticle production in hadron-hadron collision. This model treats the soft and hard component of hadron production in a unified way. The basis for the model is the unitarization of the soft and hard cross sections.

The first results of the model presented here indicate that the model has the potential to describe all features of hadron production known at present, and the model makes detailed predictions at the energies of future hadron colliders.

The model as presented here is only the first version of a model, which will be completed in many respects, we mention only: diffractive events, initial and

final state parton evolution, use of alternative fragmentation codes, working out the predictions of the model beyond the leading log approximation and applying the model to study the correlation between the soft hadron production and other types of hard collisions.

9. Acknowledgements

One of the authors (J. R.) would like to thank Prof. M. Tigner for an invitation to the SSC-Central Design Group, where the code DTUJET-87 was written. He thanks especially Prof. D. Groom for discussions and a fruitful collaboration at the SSC-CDG, and Dr. W. R. Nelson for continuous help in using the computer facilities at SLAC. He also thanks Dr. T. Sjöstrand for a copy of the PYTHIA code and the permission to use it within DTUJET.

REFERENCES

1. A. Capella and J. Tran Thanh Van, Z. Phys. C10, 249 (1981); Phys. Lett. 114B, 450 (1982).
2. P. Aurenche and F. W. Bopp, Z. Phys. C13, 205 (1982); Phys. Lett. 114B, 363 (1982).
3. A. B. Kaidalov, Phys. Lett. 116B, 459 (1982), A. B. Kaidalov and K. A. Ter-Martirosyan, Phys. Lett. 117B, 247 (1982).
4. J. Ranft, P. Aurenche and F. W. Bopp, Z. Phys. C26, 279 (1984); P. Aurenche, F. W. Bopp and J. Ranft, Z. Phys. C23, 67 (1984); P. Aurenche, F. W. Bopp and J. Ranft, Phys. Lett. 147B, 212 (1984).
5. P. Aurenche, F. W. Bopp and J. Ranft, Phys. Rev. D33, 1867 (1986).
6. G. Arnison et al., UA1 Collaboration, Phys. Lett. 118B, 167 (1982).
7. UA1 Collaboration, presented by F. Ceradini at the Europhysics Conference on High Energy Physics, Bari 1985.
8. C.-E. Wulz, UA1 Collaboration CERN-preprint CERN-EP/82-84 (1987).
9. P. Aurenche, F. W. Bopp and J. Ranft, Contribution to the Workshop on Physics Simulations at High Energy, Madison, Wisconsin 1986, Annecy preprint LAPP-TH-161 (1986).
10. A. Capella, J. Tran Thanh Van and J. Kwiecinski, Phys. Rev. Lett. 58, 2015 (1987).
11. J. Durand and H. Pi, Phys. Rev. Lett. 58, 303 (1987).
12. J. Ranft, SSC-report SSC-150 (1987).
13. P. Aurenche and L. González-Mestres, Phys. Rev. D18, 2995 (1978); C. B. Chin and S. Matsuda, Nucl. Phys. B134, 463 (1978).
14. L. González-Mestres and P. Aurenche, Z. Phys. C2, 229 (1979).
15. V. A. Abramovski, V. N. Gribov and O. V. Kancheli, Yad. Phys. 18, 595 (1971).
16. B. L. Combridge, J. Kripfgans and J. Ranft, Phys. Lett. 70B, 234 (1977).
17. L. V. Gribov, E. M. Levin and M. G. Ryskin, Phys. Reports 100, 1 (1983).
18. A. H. Mueller, contribution to the Division of Particles and Fields Meeting, Eugene (1985).
19. E. Eichten, I. Hinchliffe, K. Lane and C. Quigg, Rev. Mod. Phys. 56, 579 (1984); Rev. Mod. Phys. 58, 1065 (1986).
20. J. C. Collins, Illinois Tech. preprint 86–0298 (1986).

21. W. -K. Tung, preprint Fermilab-Conf-86/153T (1986) presented at the Snowmass Meeting, 1986.

22. J. P. Ralston and D. W. McKay, preprint Fermilab-PUB-86/95T (1986), Presented at the Workshop on Physics Simulations at High Energy, Madison (1986).

23. M. M. Block and R. N. Cahn, Rev. Mod. Phys. 57, 563 (1985).

24. H. U. Bengtson and G. Ingelman, Comp. Phys. Commun. 34, 251 (1985); T. Sjöstrand and M. van Zijl, Phys. Rev. D36, 2019 (1987).

25. A. Capella, U. Sukhatme and J. Tran Thanh Van, Z. Phys. C3, 329 (1980); A. B. Kaidalov, Pis'ma Zh. Esp. Teuv. Fiz. 32, 494 (1980); Yad. Fiz. 33, 1369 (1981).

26. S. Ritter and J. Ranft, Acta Phys. Polonica B11, 259 (1980); S. Ritter, Z. Phys. C6, 27 (1982); Comp. Phys. Commun. 31, 393 (1984).

27. K. Hänßgen and S. Ritter, Comp. Phys. Commun. 31, 411 (1984).

28. C. de Marzo et al. Phys. Rev. D26, 1019 (1982).

29. G. J. Alner et al., UA-5 Collaboration, Z. Phys. C33, 1 (1986).

30. G. Arnison et al.,UA-1 Collaboration, Phys. Lett. 118B, 167 (1982).

31. Z. Kola, H.B. Nielsen, P. Olsen, Nucl. Phys. B40, 317 (1970).

32. K. A. Tev-Martirosyan, Phys. Lett. 44B, 377 (1973).

33. G. J. Alner et al., UA-5 Collaboration, Phys. Lett. 138B, 304 (1984).

34. D. E. Groom, SSC-Report SSC-N-154 (1986).

35. A. D. Martin, R. G. Roberts and W.J. Stirling, Preprint, Rutherford Appleton Laboratory RAL-87-052 (1987).

Table 1

Energy fractions carried by the partons or strings corresponding to three different mechanisms: soft sea chains (ss), soft valence chains (sv) and hard chains (h). The energy fractions were obtained by sampling between 200 and 2000 events at each energy.

$\sqrt{s}$ (GeV)	E_{ss}/E_o	E_{sv}/E_o	E_h/E_o
200	0.020	0.944	0.036
540	0.036	0.925	0.039
900	0.043	0.920	0.037
2000	0.055	0.905	0.040
16000	0.071	0.883	0.046
40000	0.070	0.886	0.044

Table 2

Model results for average charged and total multiplicities in non-diffractive inelastic collisions. The charged and total multiplicities include all charged and neutral hadrons from the pseudoscalar meson octet and the baryon octet and some photons resulting from the decay of hadron resonances.

$\sqrt{s}$ (GeV)	Total Events		Soft Sea Strings		Soft Valence Strings		Hard Strings	
	$n_{\rm tot}$	$n_{\rm ch}$	$n_{\rm tot}$	$n_{\rm ch}$	$n_{\rm tot}$	$n_{\rm ch}$	$n_{\rm tot}$	$n_{\rm ch}$
53	24.4	14.1	0.36	0.21	22.7	13.11	1.28	0.74
200	41.0	23.8	2.72	1.58	34.3	19.94	4.03	2.33
540	58.9	34.1	7.55	4.40	43.1	25.1	8.26	4.83
900	69.8	40.5	11.9	6.93	47.7	27.7	10.6	6.20
2000	88.8	51.7	18.4	10.8	54.6	31.8	15.2	8.8
40000	185.3	107.6	57.0	33.1	83.2	48.3	45.2	26.0

Table 3

Particle composition at 40 TeV $\bar{p}p$ collisions.

Particle	Multiplicity	Energy Fraction
P	2.02	0.0600
$\overline{p}$	2.01	0.0612
γ	7.20	0.0191
n	1.78	0.0379
$\overline{n}$	1.81	0.0381
K_L^0	0.25	0.0010
π^+	45.7	0.2059
π^-	45.7	0.2101
K^+	5.7	0.0296
K^-	5.7	0.0315
Λ	0.84	0.0120
$\overline{\Lambda}$	0.83	0.0100
K_s^0	0.25	0.0010
Σ^-	0.17	0.0010
Σ^+	0.17	0.0023
Σ^0	0.14	0.0016
π^0	53.6	0.2114
K^0	5.37	0.0288
K^{-0}	5.34	0.0299

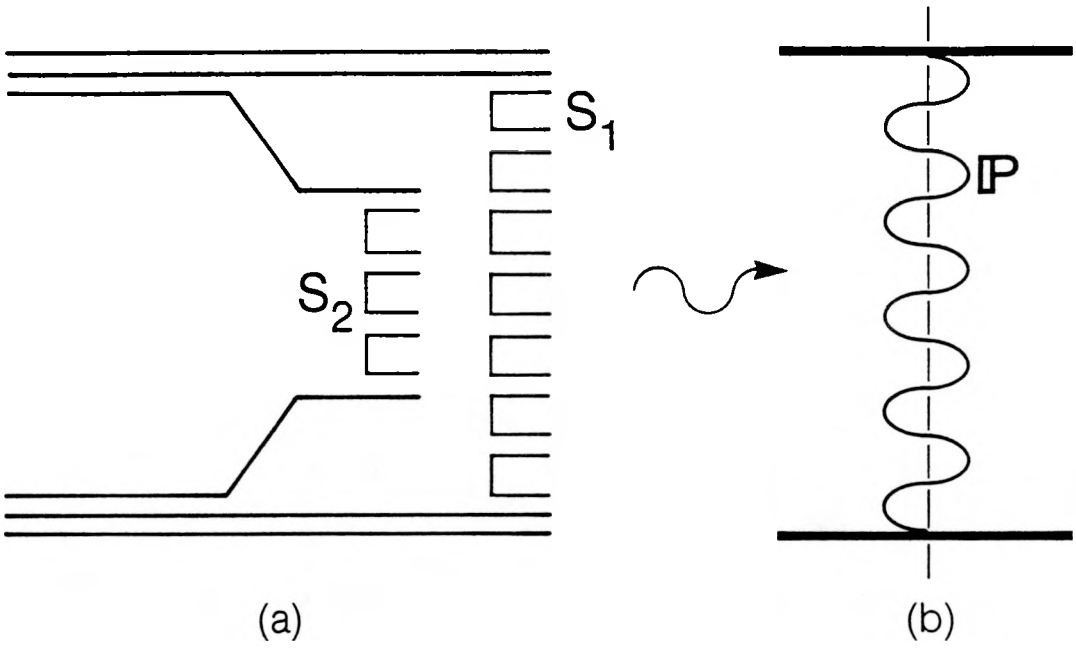

XBL 8712-5765

Fig. 1 The *s*-channel content a) of the imaginary part of the Pomeron exchange in the elastic amplitude b).

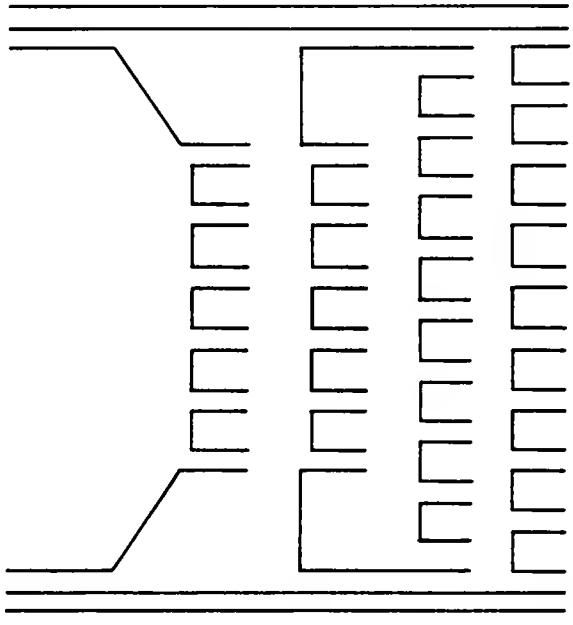

XBL 8712-5764

Fig. 2 Production of four strings in proton-antiproton interaction.

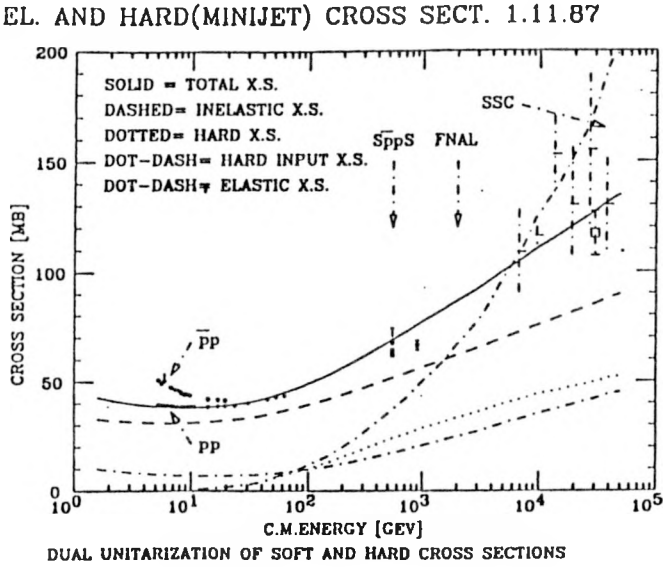

Fig. 3a σ_{total}, $\sigma_{inelastic}$ and the minijet cross section $\sigma_{h,inel}$ as calculated by the unitarization of hard and soft cross sections. We show also the input perturbative hard cross section σ_h for the production of minijets with $p_\perp$ > 2 GeV/c. The total cross section calculated is compared with data at accelerator and cosmic ray energies compiled by Groom [34]. Calculated with soft cross sections σ_s which rise with energy as given in (4) and (5) [10].

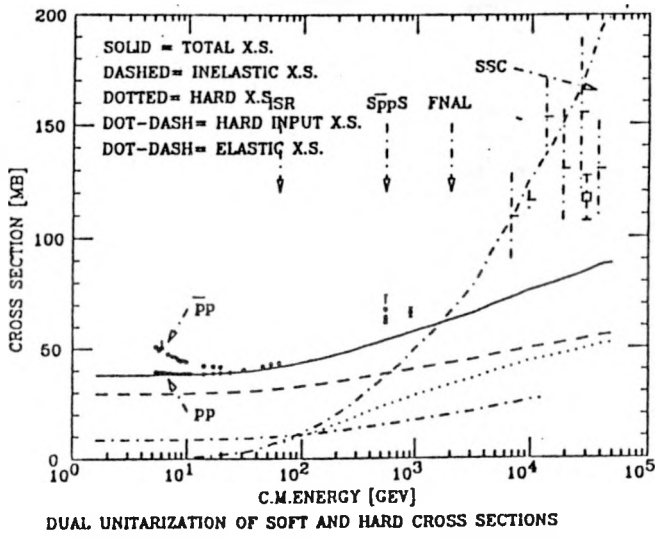

Fig. 3b σ_{total}, $\sigma_{inelastic}$ and the minijet cross section $\sigma_{h,inel}$ as calculated by the unitarization of hard and soft cross sections. We show also the input perturbative hard cross section σ_h for the production of minijets with $p_\perp$ > 2 GeV/c. The total cross section calculated is compared with data at accelerator and cosmic ray energies compiled by Groom [34]. Calculated with energy independent soft cross section σ_s as given in (6) [11].

SAMPLE DISTRIBUTION FOR L SOFT AND M HARD POMERONS
AT ECM= 316.23 S= 100000.0

0	0	0	0	0	0	0	0	0	0	0	0	0	0	0	0	0	0	0	0	0	0
1	405	144	22	7	1	0	0	0	0	0	0	0	0	0	0	0	0	0	0	0	0
2	136	56	25	6	0	0	0	0	0	0	0	0	0	0	0	0	0	0	0	0	0
3	60	24	8	3	1	1	0	0	0	0	0	0	0	0	0	0	0	0	0	0	0
4	32	17	7	4	1	0	0	0	0	0	0	0	0	0	0	0	0	0	0	0	0
5	7	8	8	2	0	0	0	0	0	0	0	0	0	0	0	0	0	0	0	0	0
6	3	1	5	0	0	0	0	0	0	0	0	0	0	0	0	0	0	0	0	0	0
7	2	1	0	1	0	0	0	0	0	0	0	0	0	0	0	0	0	0	0	0	0
8	0	0	1	0	0	0	0	0	0	0	0	0	0	0	0	0	0	0	0	0	0
9	1	0	0	0	0	0	0	0	0	0	0	0	0	0	0	0	0	0	0	0	0
10	0	0	0	0	0	0	0	0	0	0	0	0	0	0	0	0	0	0	0	0	0
11	0	0	0	0	0	0	0	0	0	0	0	0	0	0	0	0	0	0	0	0	0
12	0	0	0	0	0	0	0	0	0	0	0	0	0	0	0	0	0	0	0	0	0

SAMPLE DISTRIBUTION FOR L SOFT AND M HARD POMERONS
AT ECM= 1000.00 S= 1000000.0

0	0	0	0	0	0	0	0	0	0	0	0	0	0	0	0	0	0	0	0	0	0
1	352	124	40	11	5	2	1	0	0	0	0	0	0	0	0	0	0	0	0	0	0
2	115	50	31	15	6	2	0	0	1	0	0	0	0	0	0	0	0	0	0	0	0
3	42	30	28	11	7	4	0	0	0	0	0	0	0	0	0	0	0	0	0	0	0
4	12	17	15	9	7	1	0	1	0	0	0	0	0	0	0	0	0	0	0	0	0
5	3	14	5	5	2	2	1	0	0	0	0	0	0	0	0	0	0	0	0	0	0
6	5	6	8	2	0	0	0	0	0	0	0	0	0	0	0	0	0	0	0	0	0
7	0	1	2	0	1	0	0	0	0	0	0	0	0	0	0	0	0	0	0	0	0
8	1	3	0	0	0	0	0	0	0	0	0	0	0	0	0	0	0	0	0	0	0
9	0	0	0	0	0	0	0	0	0	0	0	0	0	0	0	0	0	0	0	0	0
10	0	0	0	0	0	0	0	0	0	0	0	0	0	0	0	0	0	0	0	0	0
11	0	0	0	0	0	0	0	0	0	0	0	0	0	0	0	0	0	0	0	0	0
12	0	0	0	0	0	0	0	0	0	0	0	0	0	0	0	0	0	0	0	0	0

SAMPLE DISTRIBUTION FOR L SOFT AND M HARD POMERONS
AT ECM= 3162.28 S= 10000000.0

0	0	0	0	0	0	0	0	0	0	0	0	0	0	0	0	0	0	0	0	0	0
1	319	144	38	22	13	2	3	0	0	1	0	0	0	0	0	0	0	0	0	0	0
2	96	45	37	19	14	5	3	1	0	1	0	0	0	0	0	0	0	0	0	0	0
3	37	26	18	17	7	1	3	2	1	0	0	0	0	0	0	0	0	0	0	0	0
4	14	15	11	6	4	3	3	1	1	0	0	0	0	0	0	0	0	0	0	0	0
5	6	7	6	9	4	4	2	1	0	0	0	0	0	0	0	0	0	0	0	0	0
6	4	4	3	3	3	1	0	1	0	0	0	0	0	0	0	0	0	0	0	0	0
7	1	2	0	0	2	1	0	0	0	0	0	0	0	0	0	0	0	0	0	0	0
8	0	0	1	0	0	0	0	0	0	0	0	0	0	0	0	0	0	0	0	0	0

SAMPLE DISTRIBUTION FOR L SOFT AND M HARD POMERONS
AT ECM= 10000.00 S= 100000000.0

0	0	0	0	0	0	0	0	0	0	0	0	0	0	0	0	0	0	0	0	0	0
1	307	133	36	25	12	3	4	5	2	0	1	0	0	0	0	0	0	0	0	0	0
2	81	52	26	14	8	6	5	4	4	1	0	0	0	0	0	0	0	0	0	0	0
3	35	26	18	12	4	8	8	3	1	2	0	0	0	1	0	0	0	0	0	0	0
4	15	12	13	15	10	8	0	4	3	2	1	1	0	0	0	0	0	0	0	0	0
5	3	7	3	4	5	1	3	5	2	1	1	1	0	0	0	0	0	0	0	0	0
6	2	2	5	2	3	2	0	1	2	1	0	0	0	0	0	0	0	0	0	0	0
7	0	0	3	2	1	0	0	1	0	0	1	0	0	0	0	0	0	0	0	0	0
8	0	0	0	0	1	0	0	0	0	2	0	0	0	0	0	0	0	0	0	0	0
9	0	0	0	1	0	0	1	0	0	0	0	0	0	0	0	0	0	0	0	0	0
10	0	0	0	0	0	0	0	0	0	0	0	0	0	0	0	0	0	0	0	0	0
11	0	0	0	0	0	0	0	0	0	0	0	0	0	0	0	0	0	0	0	0	0
12	0	0	0	0	0	0	0	0	0	0	0	0	0	0	0	0	0	0	0	0	0

SAMPLE DISTRIBUTION FOR L SOFT AND M HARD POMERONS
AT ECM= 31622.78 S= 1000000000.0

0	0	0	0	0	0	0	0	0	0	0	0	0	0	0	0	0	0	0	0	0	0
1	299	97	26	12	19	2	3	4	2	1	2	0	0	0	0	0	0	0	0	0	0
2	95	44	27	15	14	6	4	4	4	3	1	1	1	0	1	0	0	0	1	0	0
3	40	20	15	14	8	6	5	1	5	5	2	2	0	1	0	1	0	0	0	0	0
4	7	12	9	7	8	9	6	5	7	1	5	2	1	1	0	0	0	0	0	0	0
5	4	3	6	8	5	8	3	3	4	2	2	1	3	1	0	0	0	0	0	0	0
6	4	2	0	3	2	5	1	5	3	1	1	1	1	0	0	0	0	0	0	0	0
7	0	0	1	1	2	2	4	2	1	3	0	0	0	1	0	0	0	0	0	0	0
8	0	0	0	0	1	0	3	0	0	1	0	1	0	0	0	0	0	0	0	0	0
9	0	0	0	0	0	0	0	0	1	0	0	0	0	0	0	0	0	0	0	0	0
10	0	0	0	0	0	0	0	0	0	0	0	0	0	0	0	0	0	0	0	0	0
11	0	0	0	0	0	0	0	0	0	1	0	0	0	0	0	0	0	0	0	0	0
12	0	0	0	0	0	0	0	0	0	0	0	0	0	0	0	0	0	0	0	0	0

Fig. 4 Distribution in the number $n_S = L$ of soft (down the page) and the number $n_H = M$ of hard (across the page) Pomerons, as calculated by sampling 1000 events at each energy for the distribution given in Appendix B.

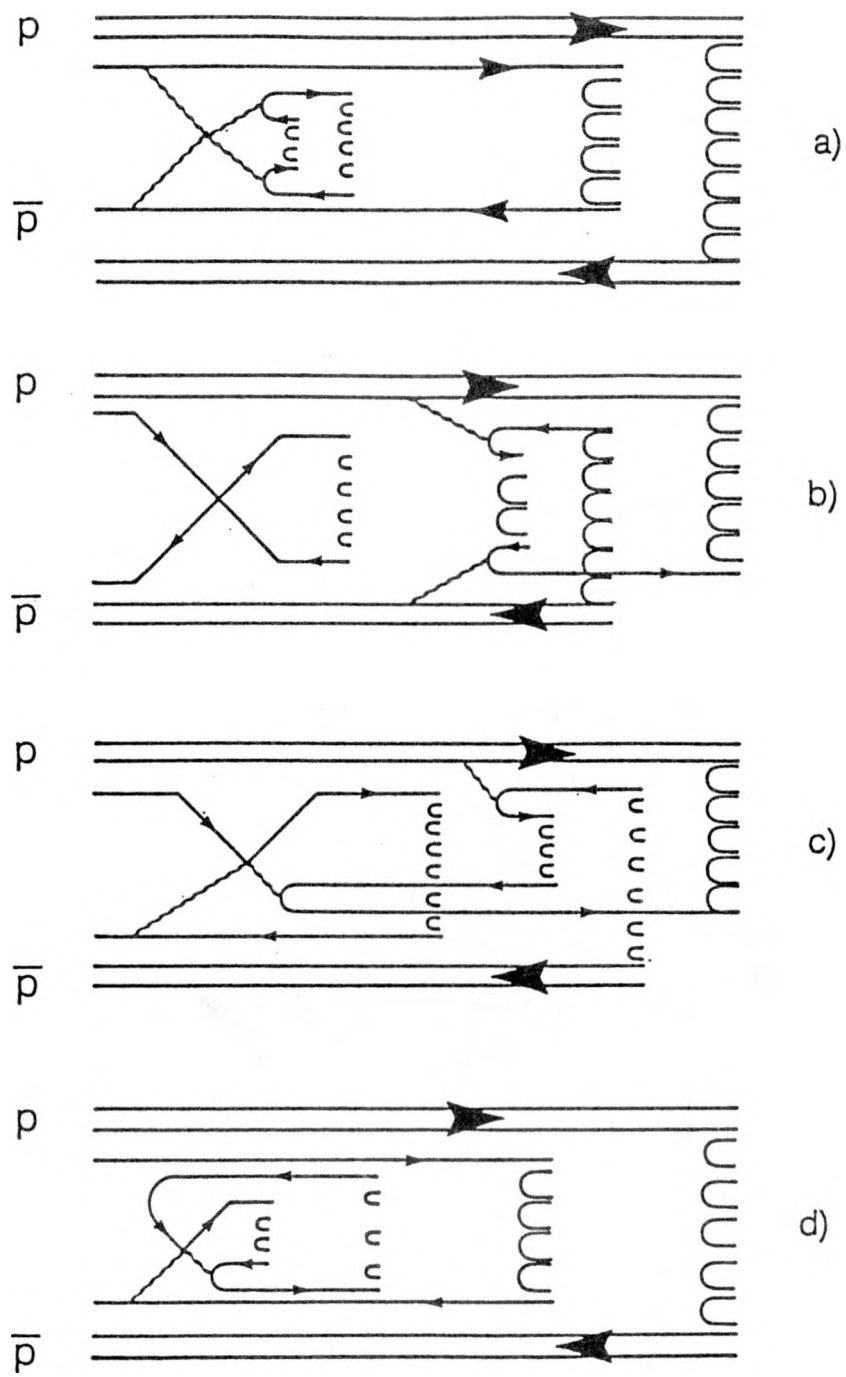

Fig. 5 Examples for string configurations in events with one soft and one hard Pomeron for different hard scattering subprocesses. a) gluon-gluon, b) valence quark-valance quark, c) valence quark-gluon and d) sea quark-gluon.

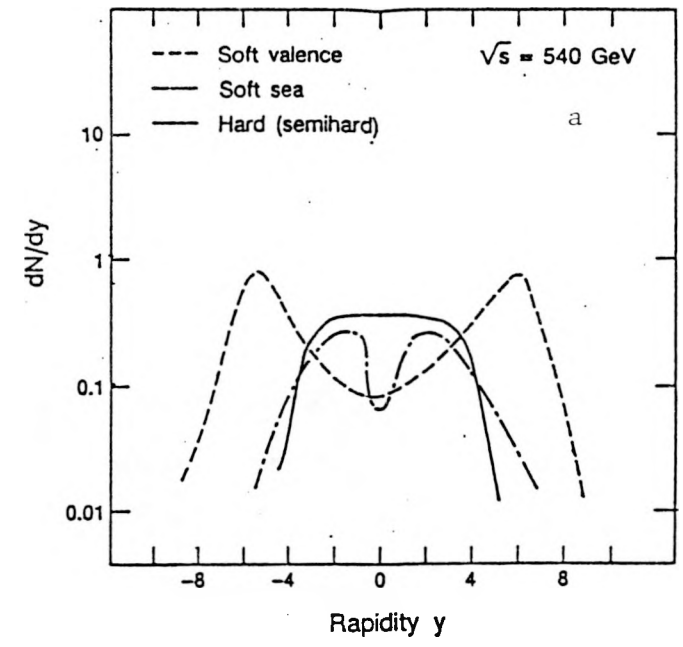

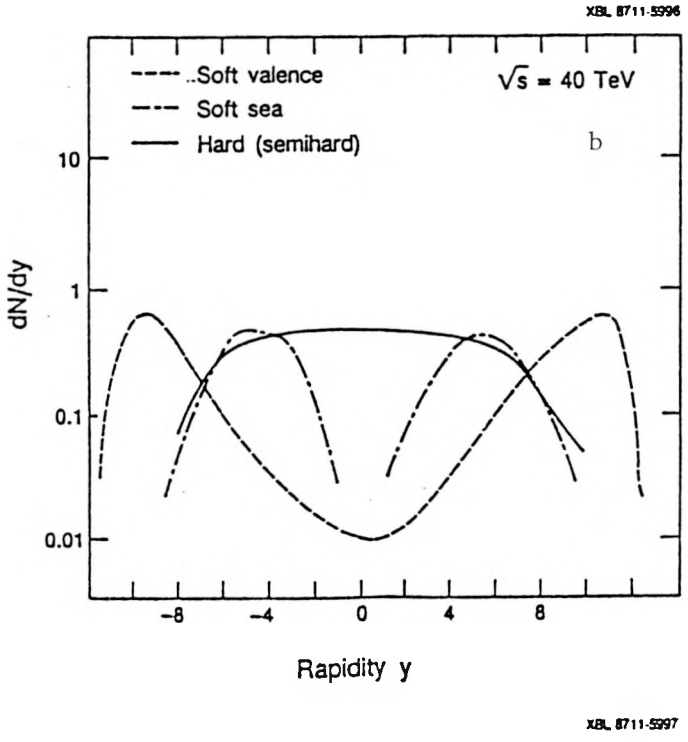

Fig. 6 Rapidity distributions of the partons at the ends of strings. We give separate curves for the three components: soft valence strings, soft sea strings and hard strings. a) at $\sqrt{s} = 540$ GeV and b) at $\sqrt{s} = 40$ TeV.

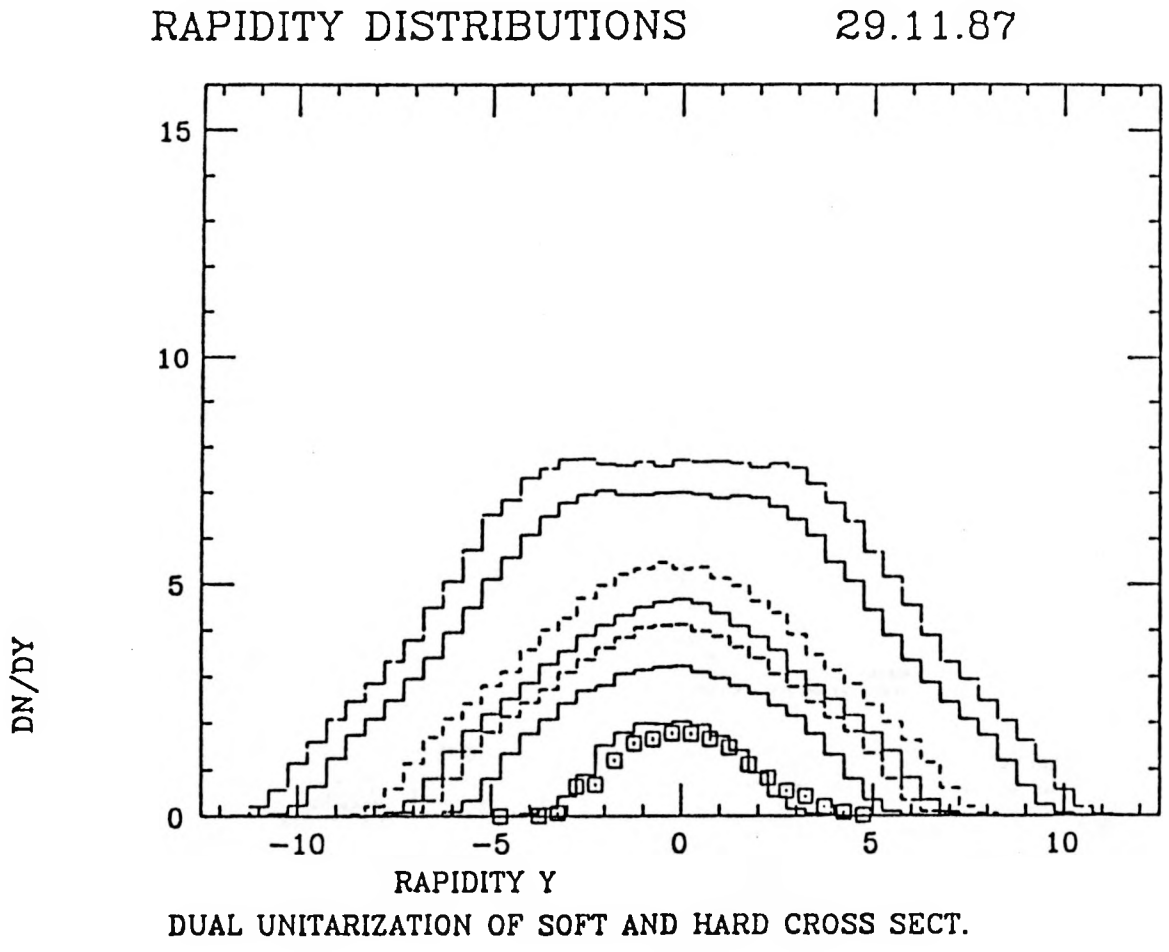

Fig. 7 Rapidity distributions of all charged particles. The histograms are for the following energies: $\sqrt{s}$ = 19.42 GeV (E_{lab} = 200 GeV), and $\sqrt{s}$ = 200, 540, 900 GeV and 2, 16 and 40 GeV. At the lowest energy we compare with data from [28].

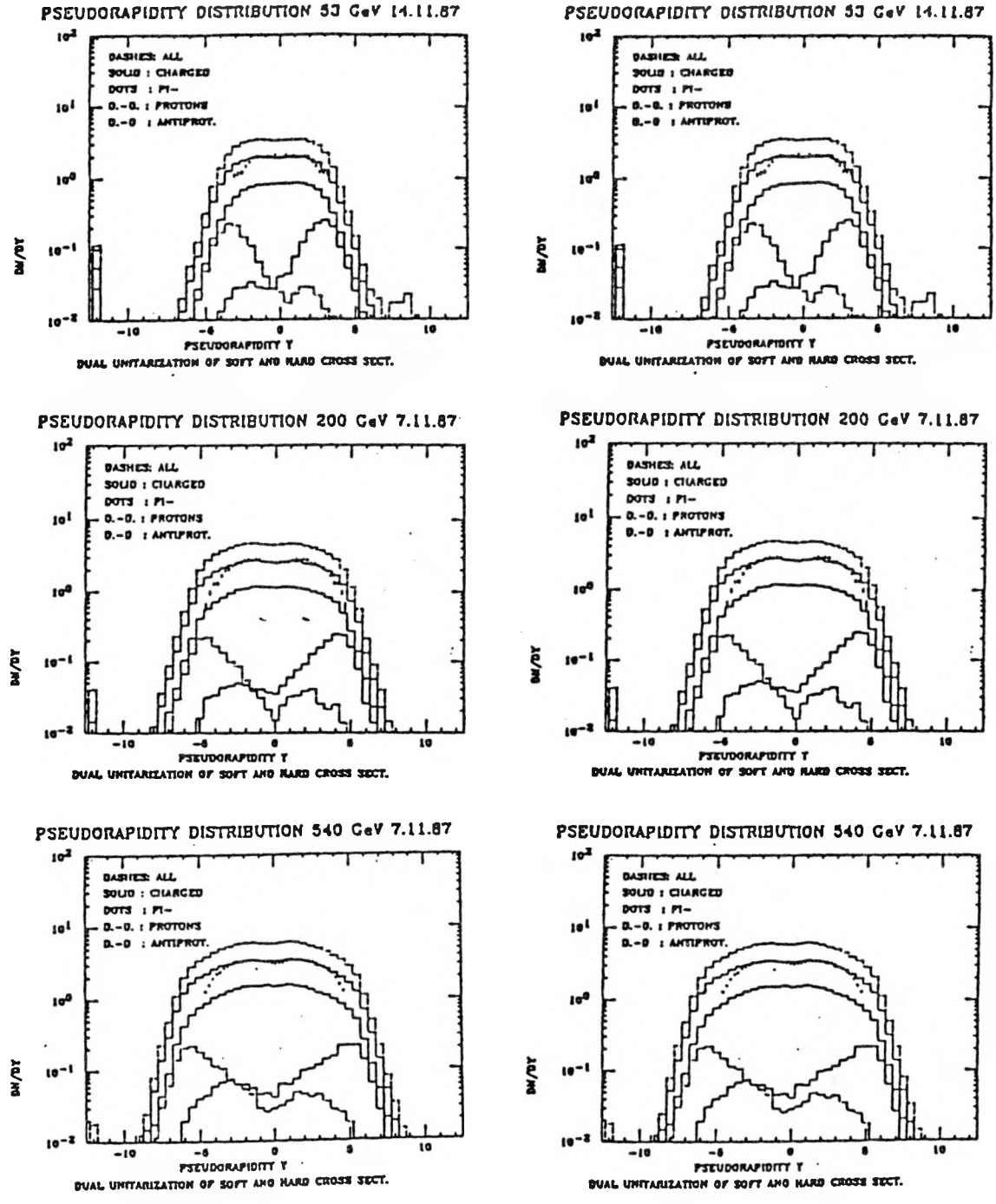

Fig. 8 Pseudorapidity distributions dN/dη calculated at ISR to SSC energies in $\bar{p}p$ collisions. The data points at energies up to $\sqrt{s} = 900$ GeV are from the UA-5 Collaboration [29]. The calculated distributions correspond to non-diffractive inelastic events.

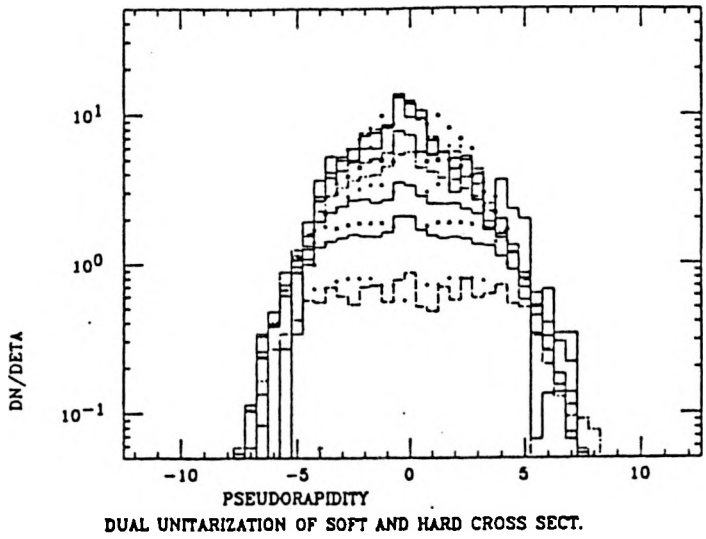

Fig. 9a Comparison of semi-inclusive pseudorapidity distributions with data from the UA-5 Collaboration [29]. a) $\sqrt{s} = 200$ GeV. The data points and histograms starting from the lowest pseudorapidity plateau are for the following ranges of the charged particle multiplicity: $2 \leq n_{ch} \leq 10$, $12 \leq n_{ch} \leq 20$, $22 \leq n_{ch} \leq 30$, $32 \leq n_{ch} \leq 40$, $42 \leq n_{ch} \leq 50$ and $n_{ch} \leq 52$.

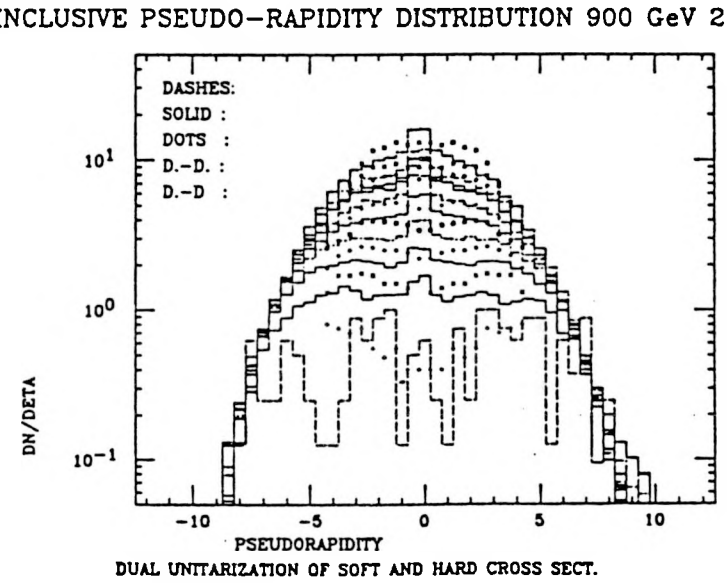

Fig. 9b Comparison of semi-inclusive pseudorapidity distributions with data from the UA-5 Collaboration [29].b) $\sqrt{s} = 900$ GeV. The data points and histograms starting from the lowest pseudorapidity plateau are for: $2 \leq n_{ch} \leq 10$, $12 \leq n_{ch} \leq 20$, $22 \leq n_{ch} \leq 30$, $32 \leq n_{ch} \leq 40$, $42 \leq 50$, $52 \leq n_{ch} \leq 60$ (no data points in this range), $62 \leq n_{ch} \leq 70$, $72 \leq n_{ch} \leq 80$, $n_{ch} \geq 82$.

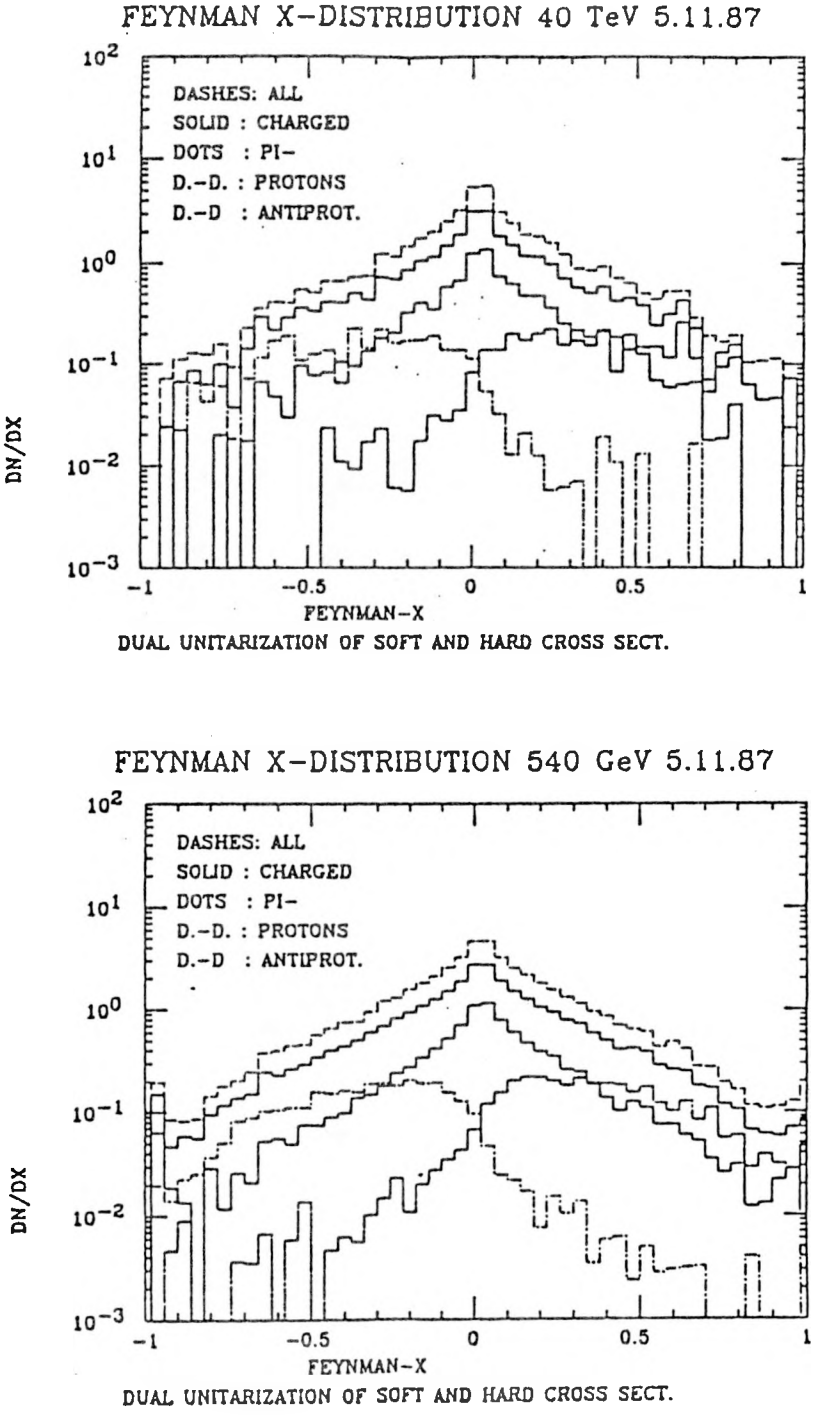

Fig. 10 Feynman-x distributions calculated for $\bar{p}p$ collisions at 540 GeV and 40 TeV. The calculated distributions correspond to nondiffractive inelastic events.

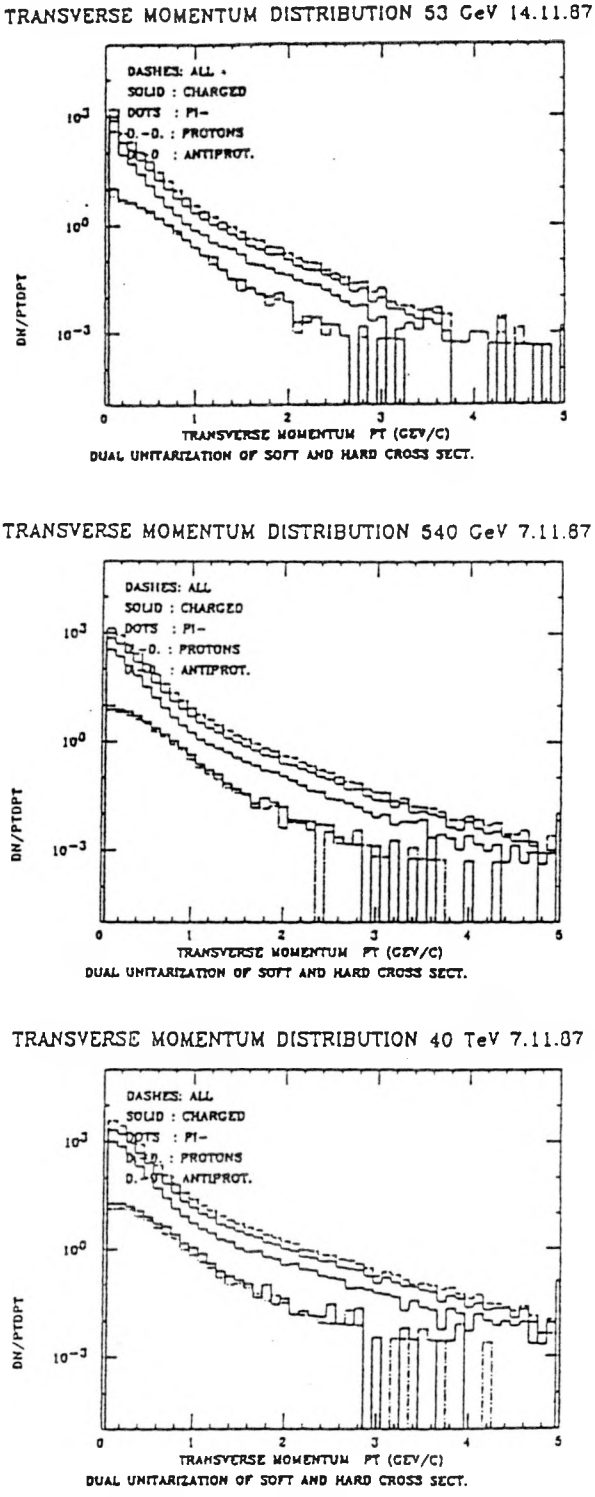

Fig. 11 Transverse momentum distributions for minimum bias events at ISR to SSC energies. The calculated distributions correspond to nondiffractive inelastic events.

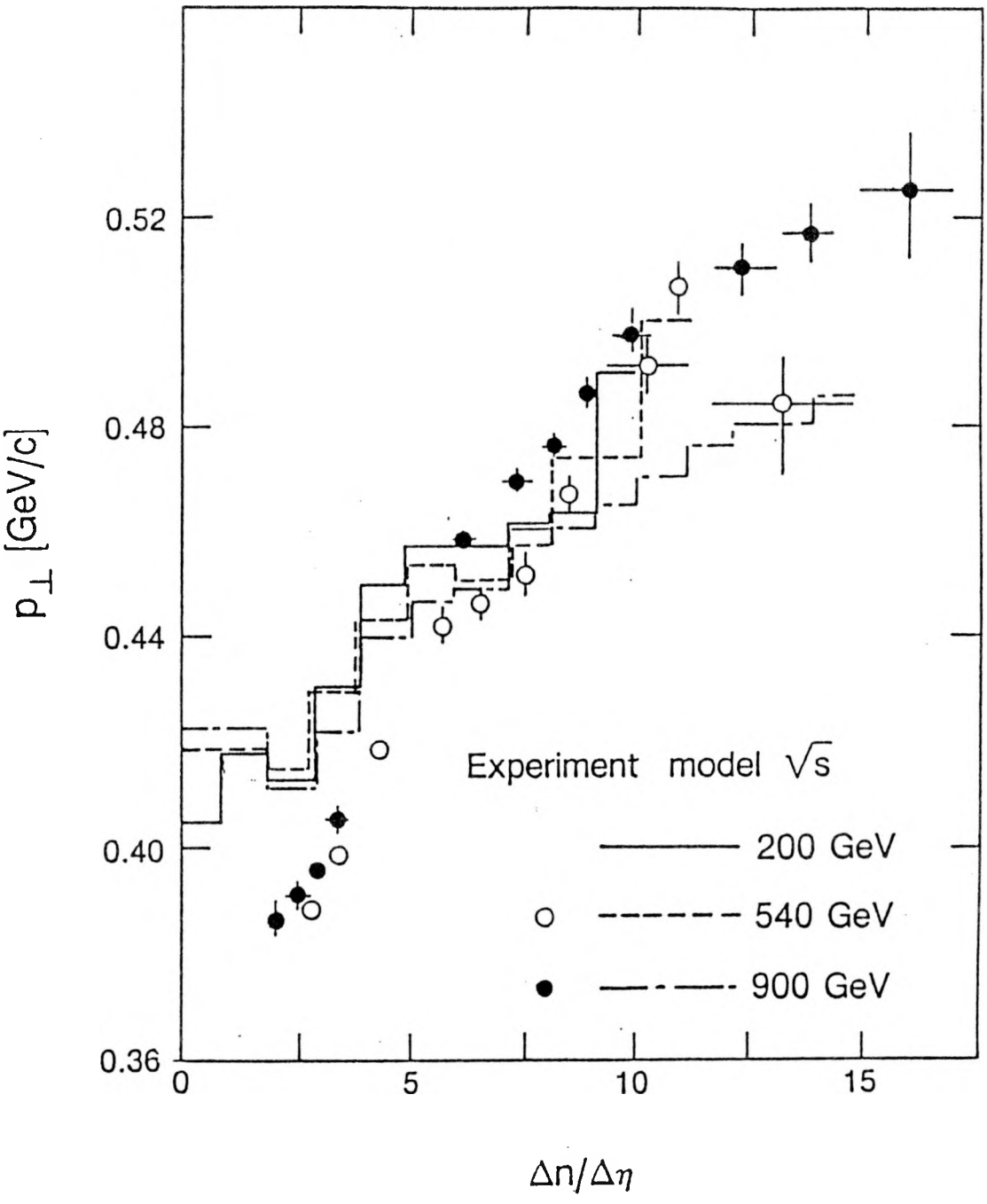

Fig. 12 Correlation between the average transverse momenta and the multiplicity per pseudorapidity interval. The model results are compared with data from the UA1-Collaboration [30].

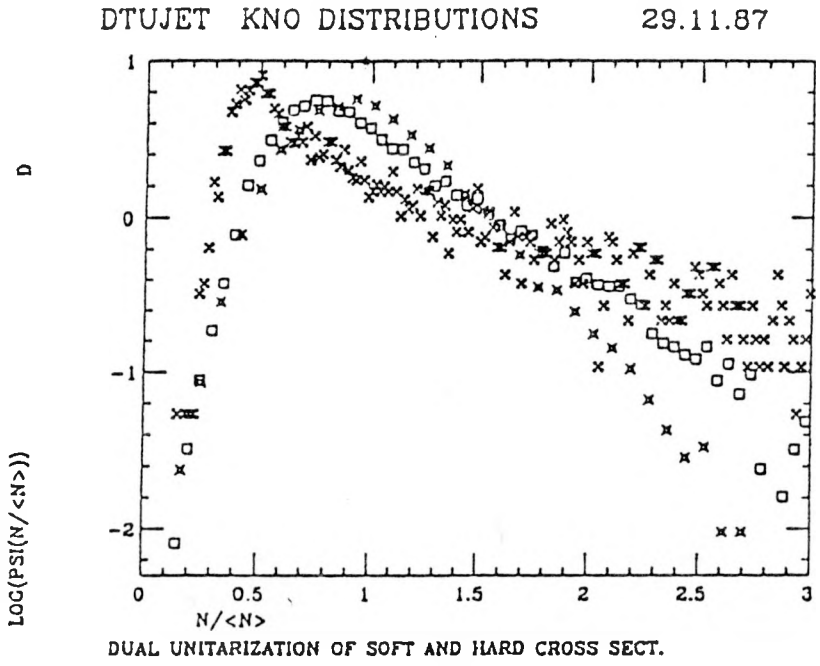

Fig. 13a KNO-multiplicity distributions of all charged particles. a) Model, ¤ $\sqrt{s}$ = 200 GeV, □ $\sqrt{s}$ = 900 GeV and × $\sqrt{s}$ = 40 TeV.

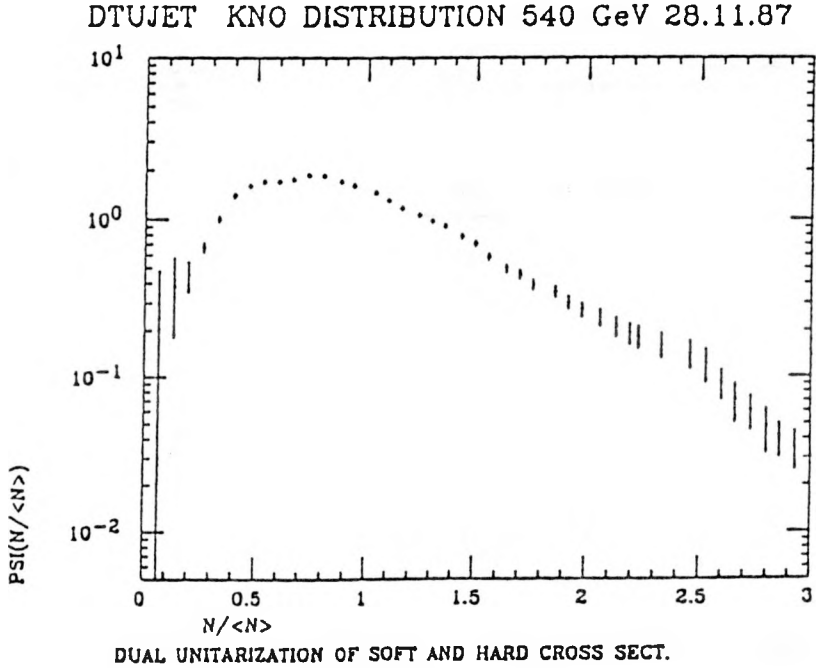

Fig. 13b KNO-multiplicity distributions of all charged particles.b) Experimental data [29] at $\sqrt{s}$ = 540 GeV.

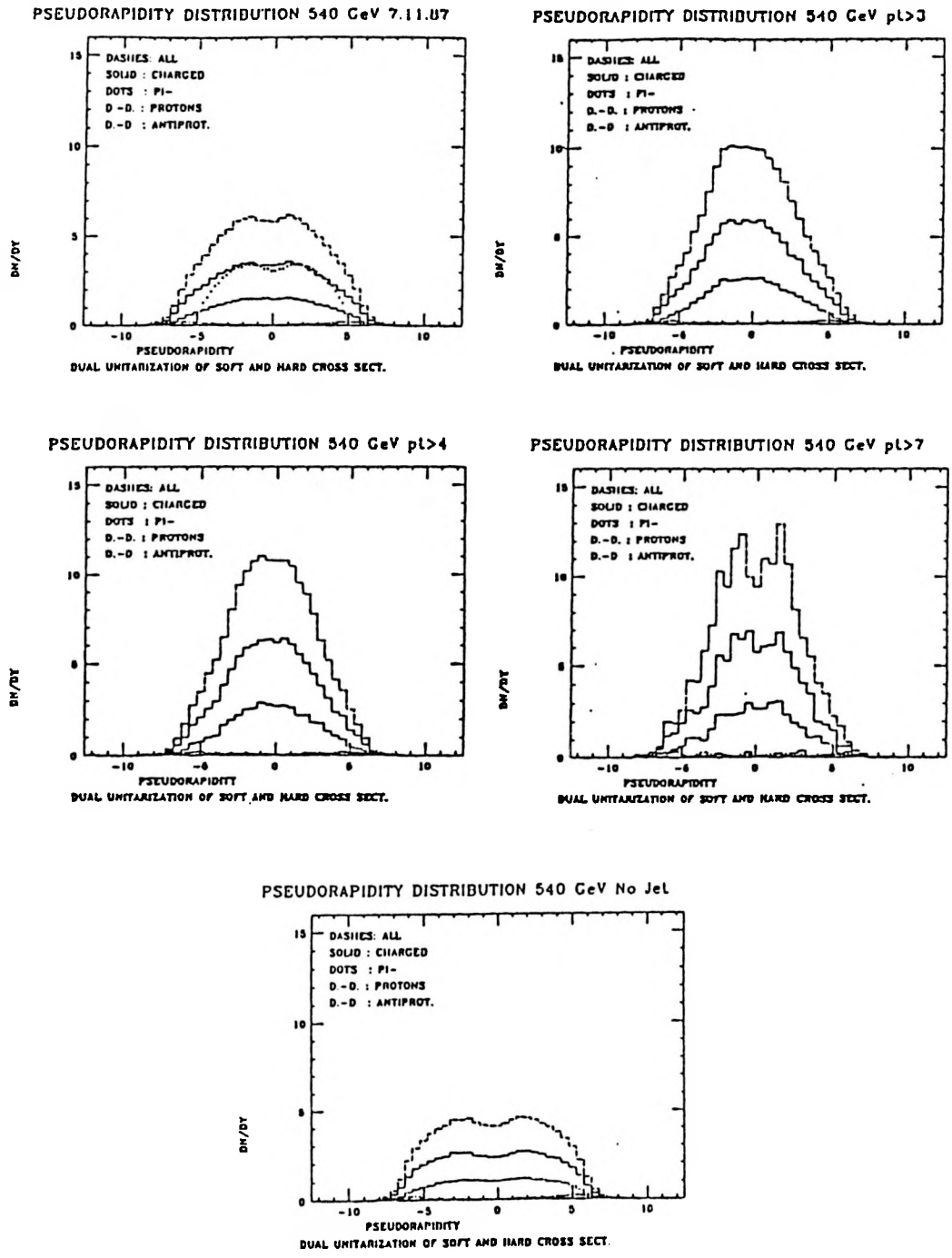

Fig. 14 Pseudorapidity distributions calculated for $\bar{p}p$ interactions at 540 GeV for minimum bias events, events with hard scattered jets with transverse momenta above a given $p_\perp$ in GeV and for events without hard jets ($n_{\hat{h}} = 0$). Hard "jets" are always the jets used in the construction of the model, not jets as determined by a jet finding algorithm from the events.

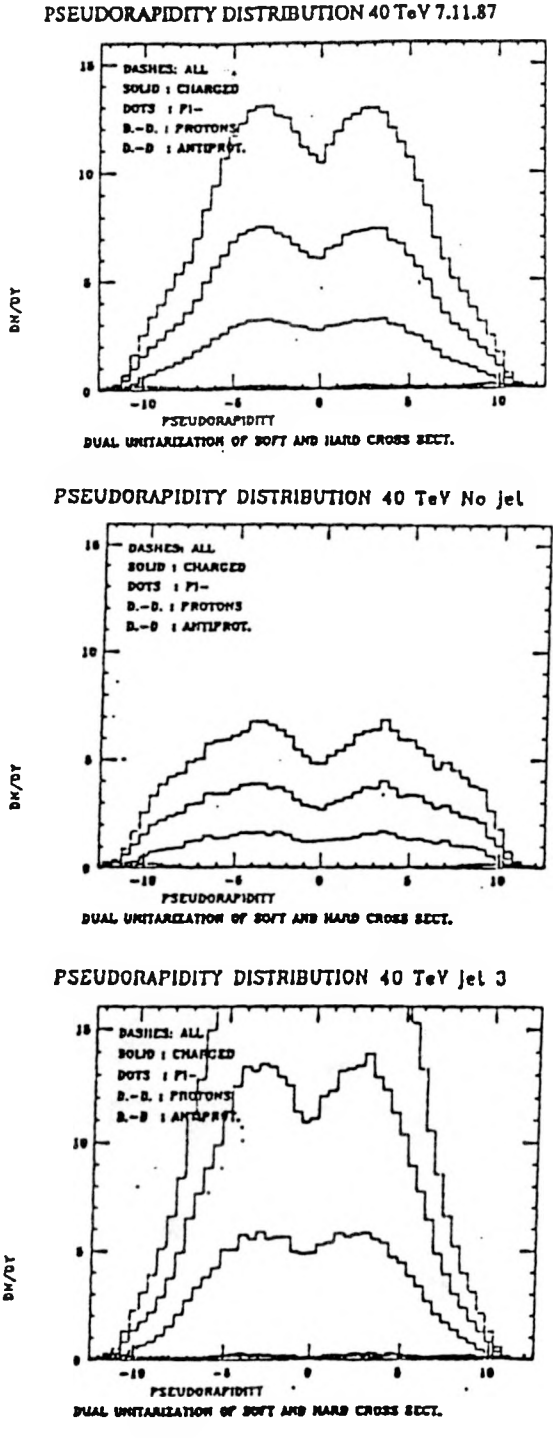

Fig. 15 Pseudorapidity distributions as given in Fig. 14 at $\sqrt{s} = 40$ TeV.

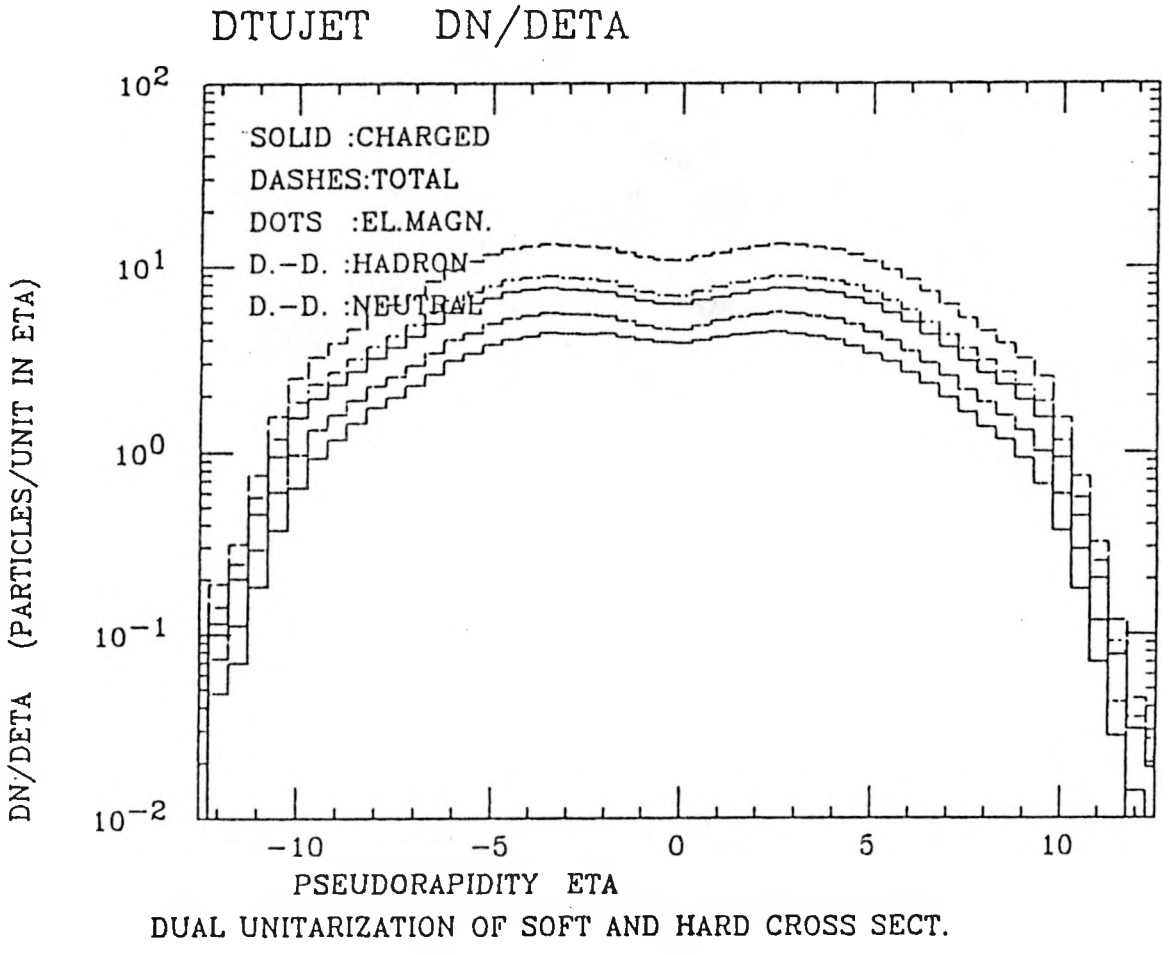

Fig. 16 Pseudorapidity distributions $dN/d\eta$ in $\bar{p}p$ collisions at 40 TeV.

Plotted are the distributions of all particles, charged particles, all hadrons, particles leading to electromagnetic cascades (π^0 and γ) and neutral particles.

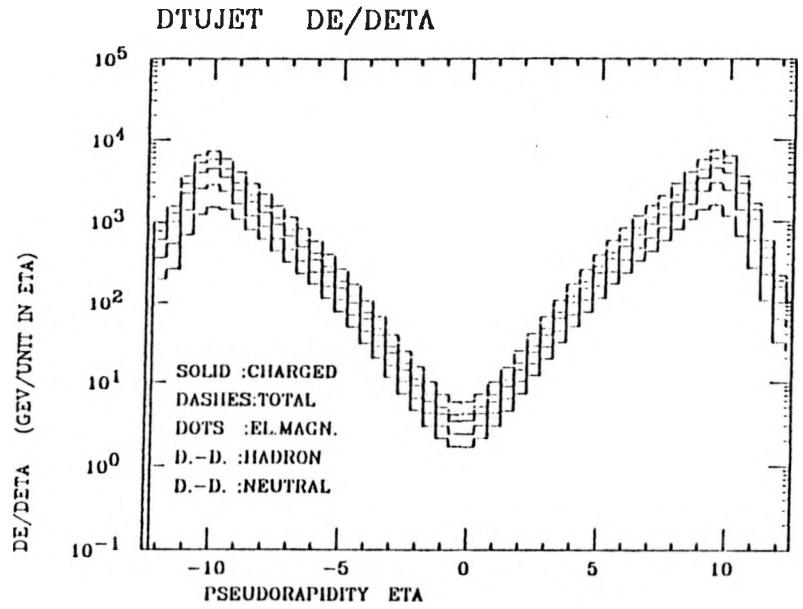

Fig. 17 Distributions $dE/d\eta$ in $\bar{p}p$ collisions at 40 TeV. Plotted for the same combinations of secondary particles as in Fig. 17.

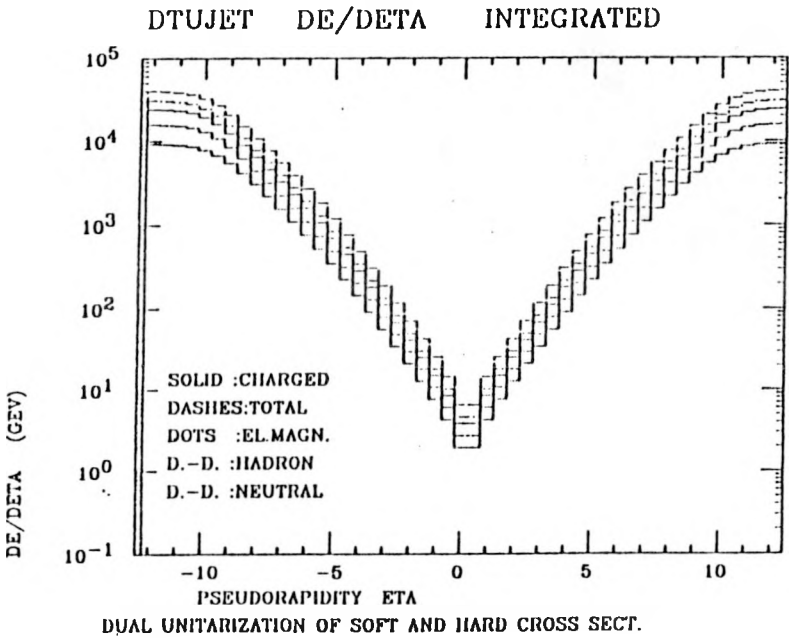

Fig. 18 Total energy within the pseudorapidity range - $\eta \leq \eta' \leq \eta$ in $\bar{p}p$ collisions at 40 TeV, plotted for the same combinations of secondaries as in Fig. 17.

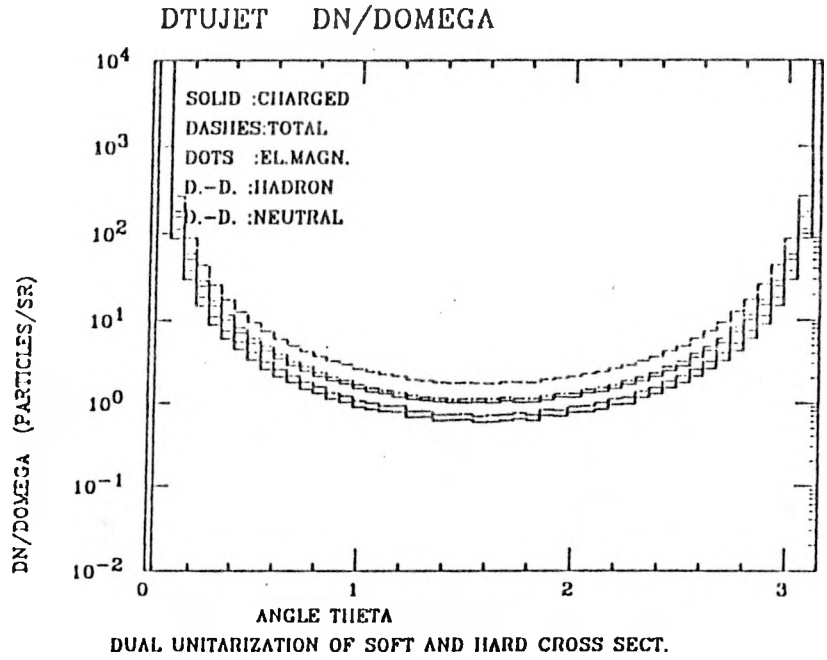

Fig. 19 The angular distribution $dN/d\Omega$ [particles per steradian] of secondaries produced in $\bar{p}p$ collisions at 40 TeV.

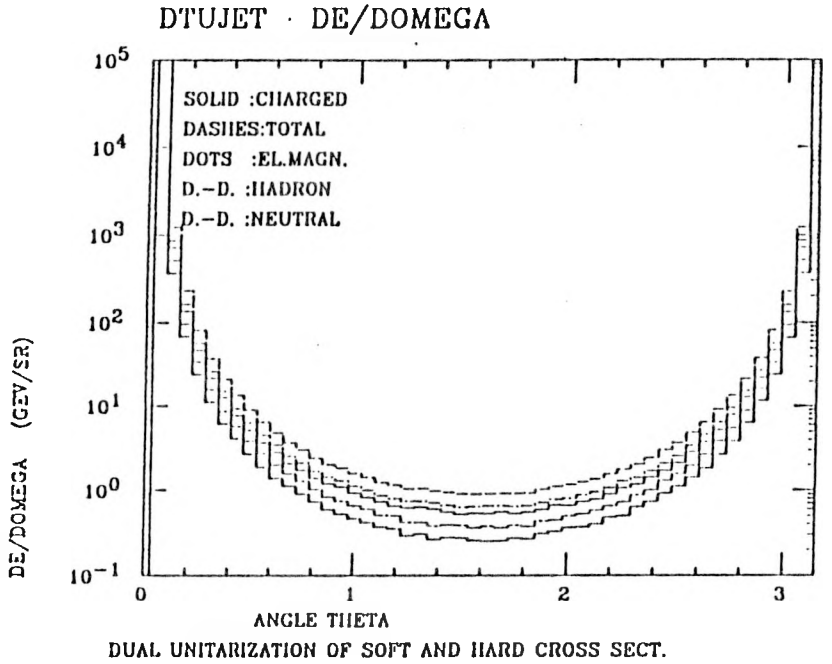

Fig. 20 The energy distribution $dE/d\Omega$ [GeV per steradian] of secondaries produced in $\bar{p}p$ collisions at 40 TeV.

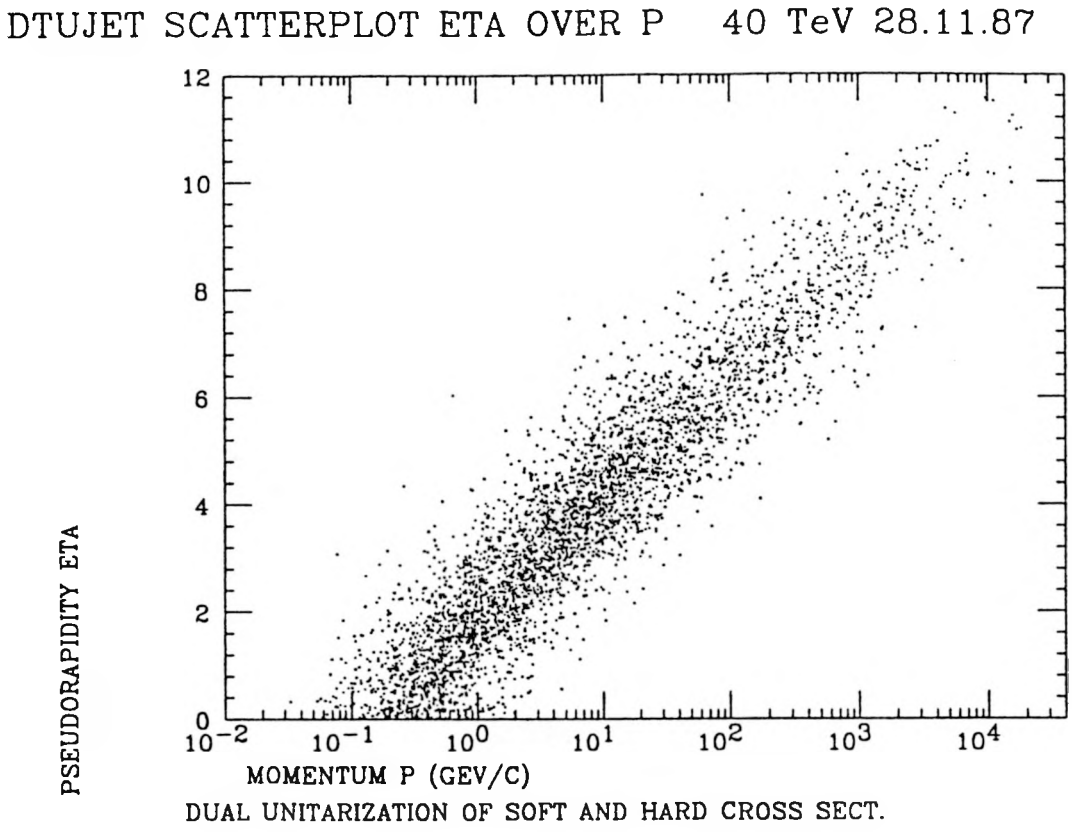

Fig. 21 Scatterplot of 4000 secondary particles produced at $\sqrt{s} = 40$ TeV in the pseudorapidity η - log p plane.

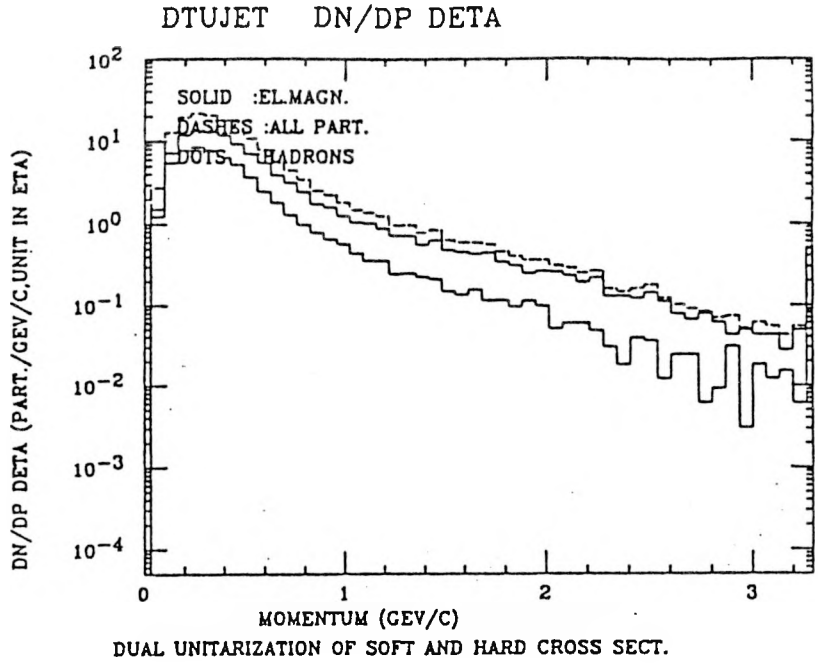

Fig. 22.1 Distributions $d^2N/dpd\eta$ [particles per GeV/c and unit of pseudorapidity]. Distributions for the rapidity bins 0.-0.5.

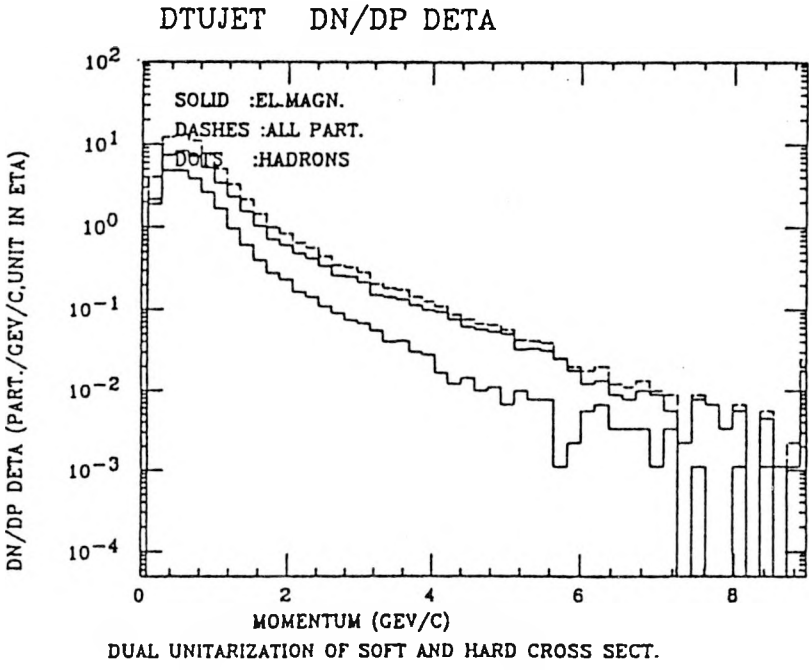

Fig. 22.2 Distributions $d^2N/dpd\eta$ [particles per GeV/c and unit of pseudorapidity]. Distributions for the rapidity bins 1.0-1.5.

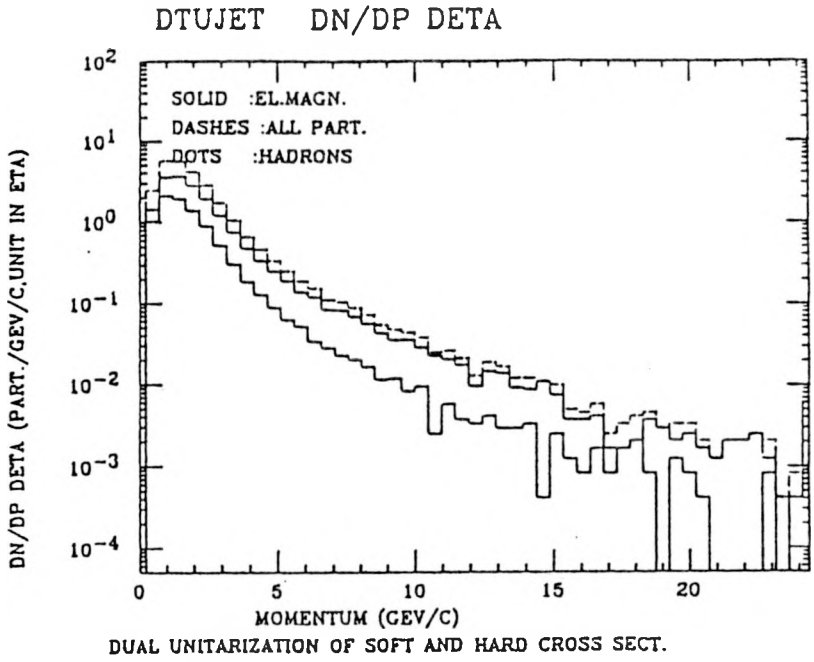

Fig. 22.3 Distributions $d^2N/dpd\eta$ [particles per GeV/c and unit of pseudorapidity]. Distributions for the rapidity bins 2.0-2.5.

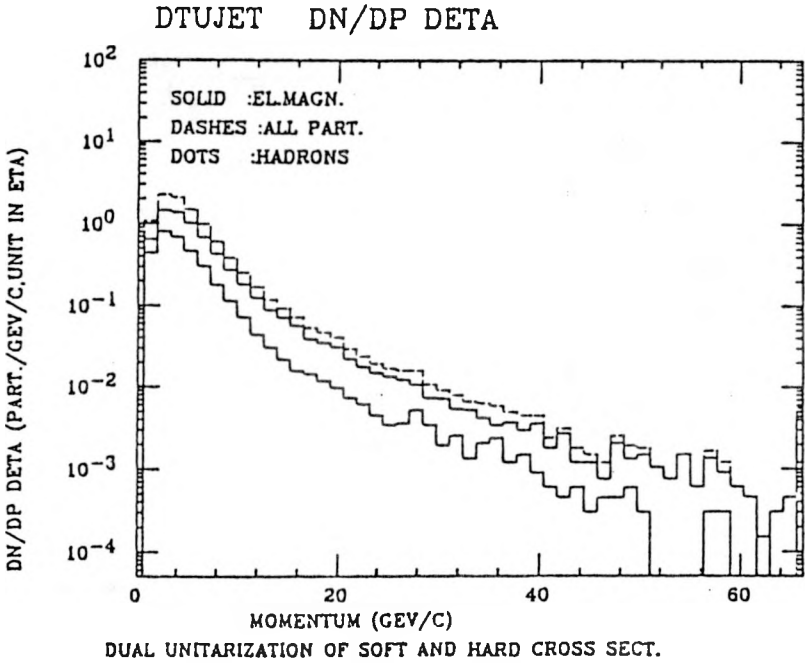

Fig. 22.4 Distributions $d^2N/dpd\eta$ [particles per GeV/c and unit of pseudorapidity]. Distributions for the rapidity bins 3.0-3.5.

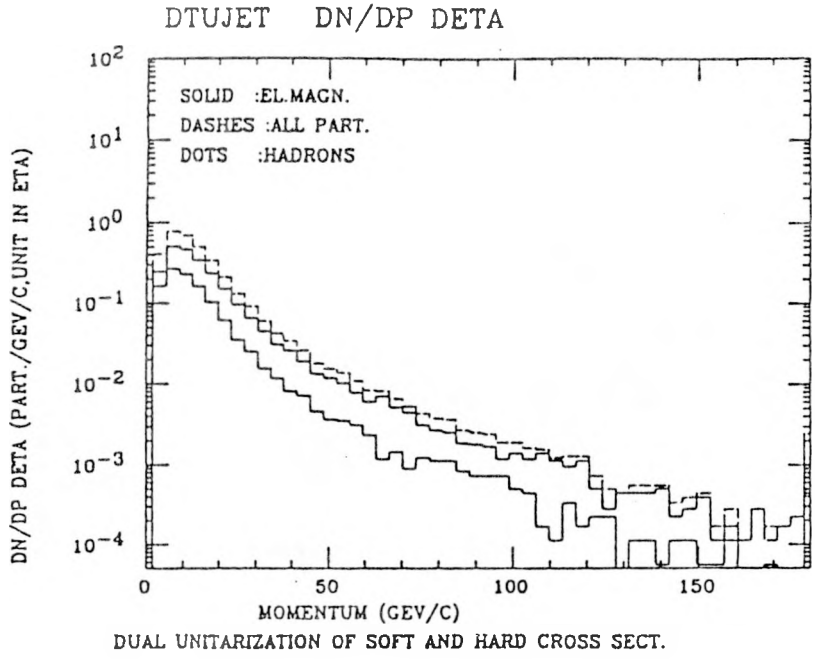

Fig. 22.5 Distributions $d^2N/dpd\eta$ [particles per GeV/c and unit of pseudorapidity]. Distributions for the rapidity bins 4.0-4.5.

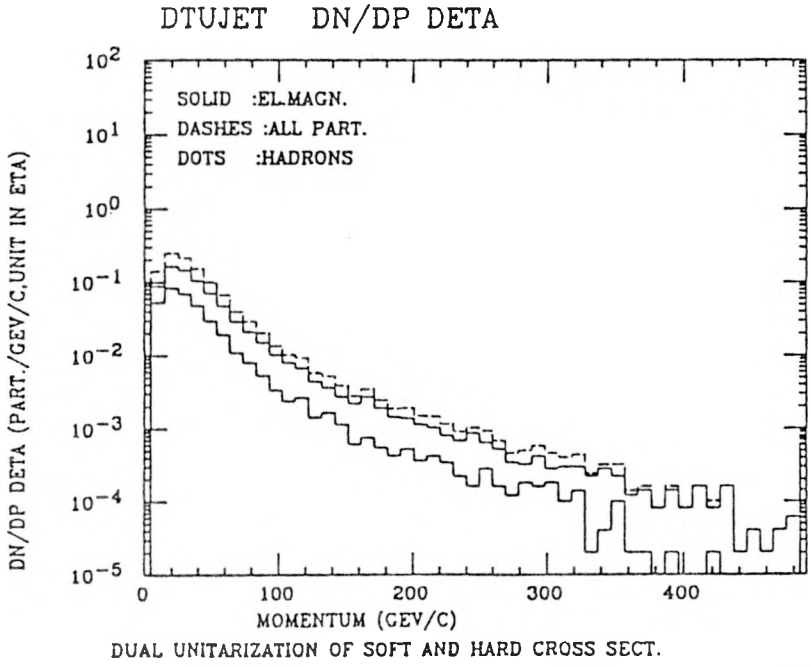

Fig. 22.6 Distributions $d^2N/dpd\eta$ [particles per GeV/c and unit of pseudorapidity]. Distributions for the rapidity bins 5.0-5.5.

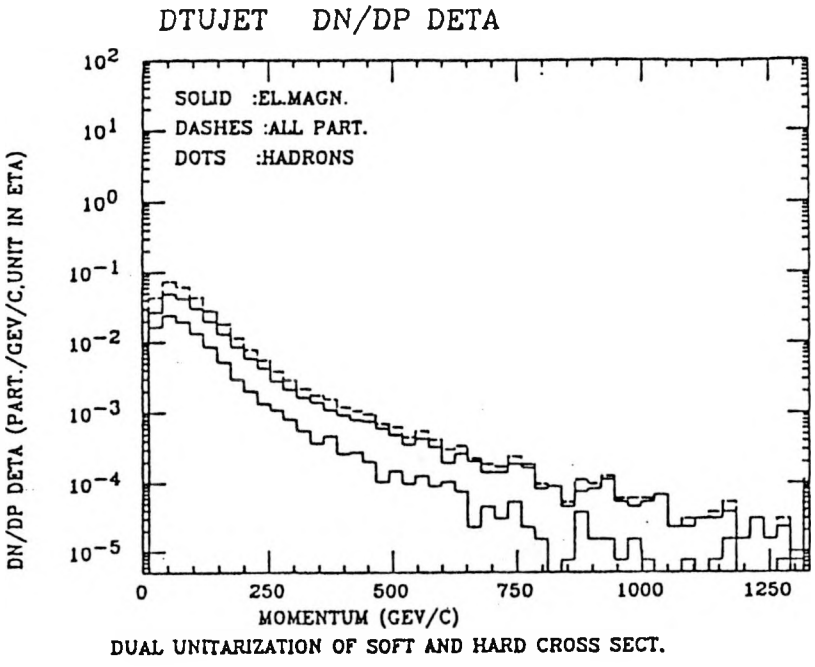

Fig. 22.7 Distributions $d^2N/dpd\eta$ [particles per GeV/c and unit of pseudorapidity]. Distributions for the rapidity bins 6.0-6.5.

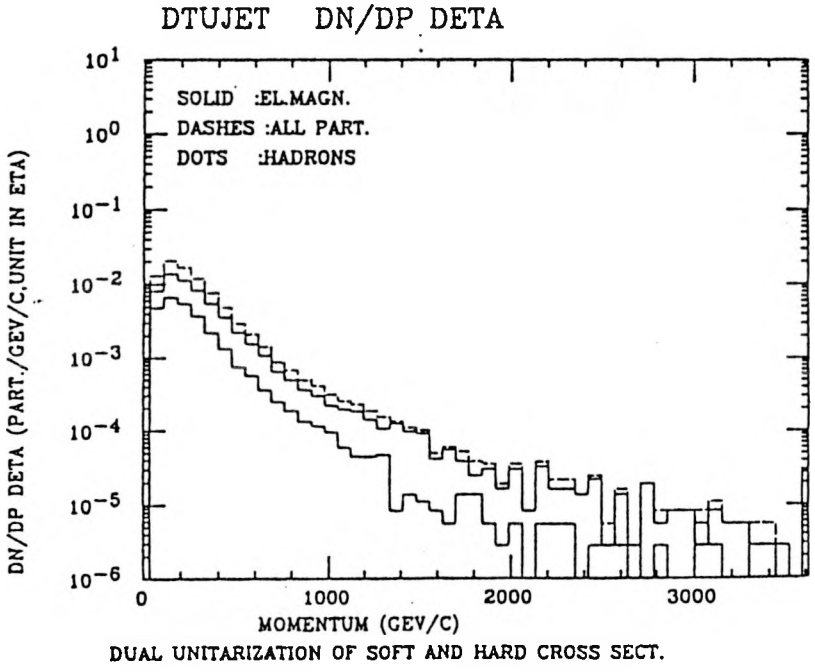

Fig. 22.8 Distributions $d^2N/dpd\eta$ [particles per GeV/c and unit of pseudorapidity]. Distributions for the rapidity bins 7.0-7.5.

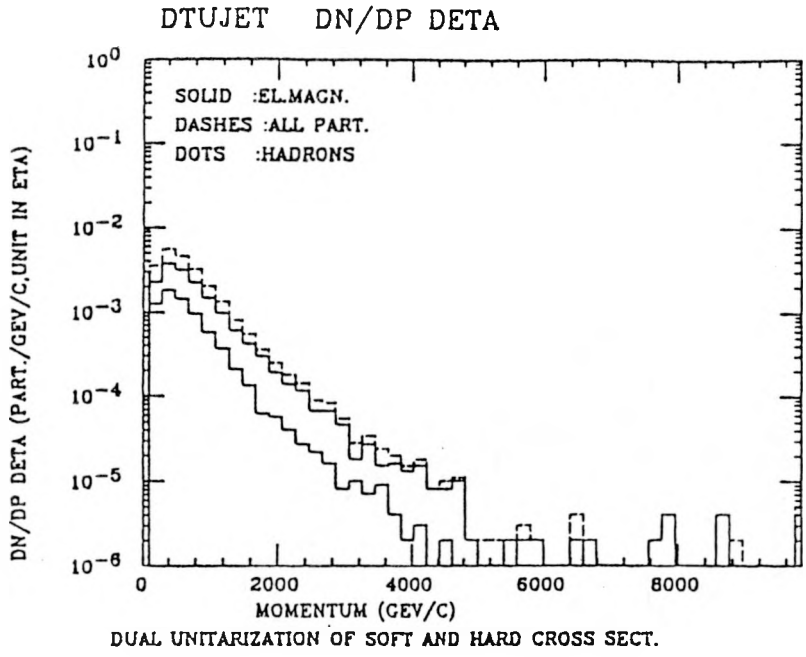

Fig. 22.9 Distributions $d^2N/dpd\eta$ [particles per GeV/c and unit of pseudorapidity]. Distributions for the rapidity bins 8.0-8.5.

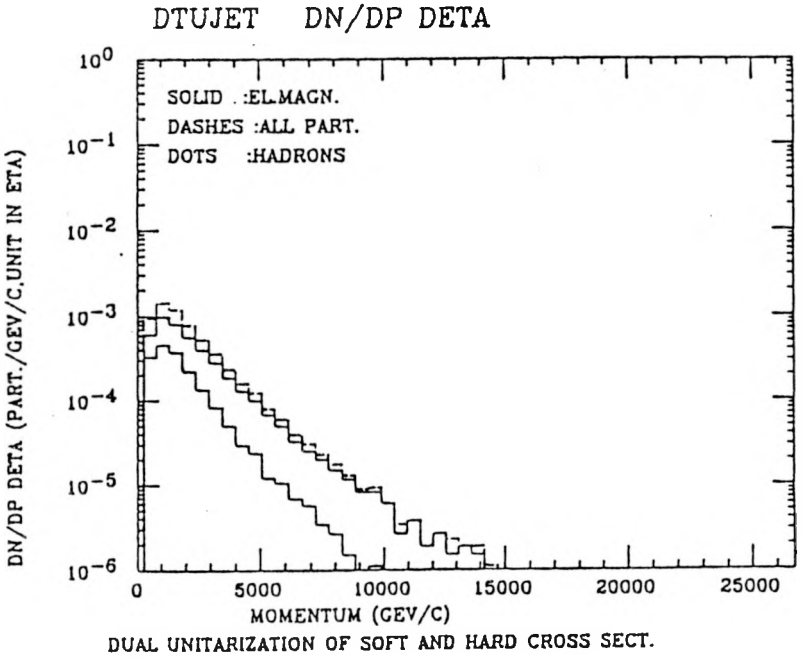

Fig.22.10 Distributions $d^2N/dpd\eta$ [particles per GeV/c and unit of pseudorapidity]. Distributions for the rapidity bins 9.0-9.5.

Appendix A

Expressions for the total and inelastic hadronic cross section as obtained by Capella et al. [10] from the cross sections σ_s (bare soft Pomeron) and σ_h (bare hard Pomeron) and a triple Pomeron contribution σ_{TP} to take diffractive events into account.

$$\sigma_{tot} = \sum_{\ell+m+n\geq 1} I_{\ell,m,n} \qquad (A-1)$$

$$\sigma_{inel} = \sum_{\ell+m+n\geq 1} 2^{\ell+m+n-1} I_{\ell,m,n} \qquad (A-2)$$

$$\sigma_D = \sum_{\ell\geq 0,\, m\geq 0,\, n\geq 1} C_n\, 2^{\ell+m+n-1} I_{\ell,m,n} \qquad (A-3)$$

$$\sigma_{h,inel} = \sum_{\ell=0, m\geq 1, n=0} 2^{\ell+m+n-1} I_{\ell,m,n} \qquad (A-4)$$

$$I_{\ell,m,n} = -\frac{8\pi}{\ell!m!n!}\left[-\frac{\sigma_s}{8\pi b_s}\right]^{\ell}\left[-\frac{\sigma_h}{8\pi b_h}\right]^{m}\left[+\frac{\sigma_{TP}}{8\pi b_{TP}}\right] \times \left[\frac{\ell}{b_s}+\frac{m}{b_h}+\frac{n}{b_{TP}}\right]^{-1} \qquad (A-5)$$

Appendix B

The cross sections for inelastic collisions with i soft Pomerons ($2i$ soft strings) and j hard Pomerons ($2j$ hard strings).

Via a resumation of the expression given in (A-2) one obtains the inelastic cross section for i soft and j hard Pomerons in the form

$$\begin{aligned}\sigma(i,j) = -\sum_{\substack{\ell'\geq 0\\(j+\ell'+n'\geq 1)}}\sum_{n'\geq 0}\sum_{\ell>\ell'}\sum_{m>j}\sum_{n\geq n'}\sum_{a=0}^{n'}\sum_{b=0}^{n'-a}\\ \times\binom{n'}{a}\binom{n'-a}{b}(-2)^a\,4^b\,2^{\ell+m+n-1}(-1)^{\ell'+j-a-b}\\ \times\binom{\ell}{\ell'}\binom{m}{j}\binom{n}{n'}I_{\ell,m,n}\,\delta_{(i-\ell'-n'-a)} \qquad (B-1)\end{aligned}$$

where $I_{\ell,m,n}$ is given by (A-5).

The formula (B-1) (in the approximation with vanishing σ_{TP} discussed in Section 4) originates from the simple formula in the impact parameter representation, which is manifestly positive and has an explicit probabilistic interpretation:

$$\sigma(i,j,B) = \frac{(2\,p_s(B))^i}{i!}\;\times\;\frac{(2\,p_h(B))^j}{j!}\exp\Big(-2\,p_s(B)-2p_h(B)\Big) \qquad (B-2)$$

where $2\,p_s(B)$ and $2\,p_h(B)$ are the corresponding bare cross-sections in the impact parameter representation normalized as

$$\begin{aligned}\int 2\,p_s(B)d^2\overrightarrow{B} &= \sigma_s\\ \int 2\,p_h(B)d^2\overrightarrow{B} &= \sigma_h \qquad (B-3)\end{aligned}$$

The formula (B-1) follows from Eq. (B-2) assuming a Gaussian shapes for $p_s(B)$ and $p_h(B)$.